Universitat
de les Illes Balears

Application of a neural mass model to study phase-amplitude coupling

Óscar Gómez Fontana

Master's Thesis

Master's degree in Physics of Complex Systems

at the

UNIVERSITAT DE LES ILLES BALEARS

Academic year *2017 - 2018*

September, 2018

UIB Master's Thesis Supervisor: Claudio R. Mirasso

Abstract

It has been shown that the amplitude of gamma oscillations modulates the phase of theta rhythm in the hippocampus [1]. In this work, we reproduce the single node Neural Mass Model (NMM) proposed in [2] to study the phase-amplitude coupling and the directionality of the oscillations in the hippocampus. The aim is to determine a particular condition of the model which can reproduce the experimental results obtained in [1]. In addition, a NMM comprised of a given number of nodes has been developed on the basis of the neural mass model proposed in [3].

Agradecimientos

Gracias...
... a Claudio por darme la oportunidad de realizar este trabajo. Su comprensión y ayuda han sido fundamentales para llevarlo a cabo.
... a Víctor por sus correos llenos de sabiduría, a él también lo considero un supervisor del trabajo.
... a mi familia de Palma, Jack, Irene y Luís, por haber podido crear un hogar entre los cuatro.
... al resto de gente que me ha acompañado este año, Alberto, Juan, Rodri, Javi, Albert, Samuel, Medea, Yolene..., por haber hecho de este año algo que recordaré con cariño.
... a mi familia por su apoyo incondicional.
... a Raquel por comprenderme, abrazarme, soportarme y sonreírme, haciendo que a su lado todo sea más fácil.

Contents

Chapter 1

Introduction

If one wonders about the earliest recorded reference to the brain, we have to travel to Egypt into the 17th century BC, where Edwin Smith Papyrus, an ancient Egyptian medical treatise contains the earliest recorded reference. In Figure 1.1 one can observe the hieroglyph for "brain", appearing in this papyrus, which describes the symptoms and diagnosis of two patients who had compound fractures of the skull [4].

Figure 1.1. Hieroglyph for the word 'brain' (c.1700 BC).

From that time on, many have tried to uncover the secrets of the brain throughout history. Nevertheless, humanity could only produce significant advances at a macroscopic level of the brain for a long time.

It was not until the 18th century when studies of the brain experienced a significant improvement. This was due to the use of the microscope and the development of a silver staining method by Camillo Golgi, which was able to show the structures of single neurons. Almost simultaneously, Santiago Ramón y Cajal, thanks to Golgi's studies, developped the neuron doctrine, which states that the neuron is the functional unit of the brain. Cajal used microscopy to discover many cell types, and also proposed functions for them, as well as drawing several sketches. An example is provided in Figure 1.2 [5].

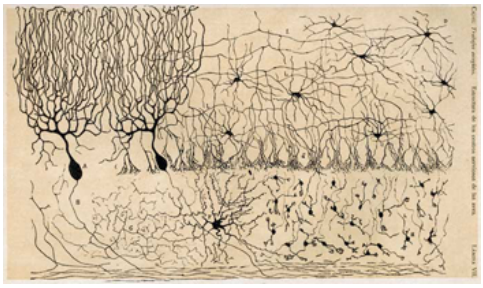

Figure 1.2. Drawings of cells in chick cerebellum by Santiago Ramón y Cajal. From [6].

At the present time of history, neuroscience is multidisciplinary field, in which efforts from neuroscientists, mathematicians, physicists and other experts are required. These joint work could lead to achieve new breakthroughs that allow humanity to have a better understanding of how the

brain functions. Particularly, computational neuroscience is a subfield of neuroscience based on developing models to integrate complex experimental data. [7].

One of the best known models is the Hodgkin and Huxley model [8], which describes at a microscopic level how action potentials in neurons are initiated and propagated. Another single-neuron level model worthwhile to point is the Izhikevich model [9], which reproduces spiking and bursting behavior of a certain type of cortical neurons, combining the biologically plausibility of Hodgkin-Huxley model and the computational efficiency of integrate-and-fire neurons.

At a mesoscopic level, we can highlight the models in which the connection between neuronal ensembles can generate oscillatory activity. This is due to the fact that the firing patterns of a group of neurons can synchronize. Additionally, the action potentials of each neuron influences the electric potential, creating a constructive interference. These synchronized firing patterns generate synchronized input into other cortical areas, which produce amplitude oscillations of the local field potential [10]. An example of mesoscopic models are the neural mass models (NMMs), which in order to facilitate the dynamic modeling, present populations consisting of a huge number of neurons with similar characteristics [11]. These models can be parameterized using experimental recorded data coming from local field potentials (LFP), electroencephalogram (EEG) or magnetoencephalograms (MEG) [12], in order to achieve a model as realistic as possible.

In addition, at a macroscopic level, we can mention that oscillatory activity can arise from interactions between different brain areas coupled through the structural connectome.

In particular, in the present work we are going to focus on the study of neural mass models. The first developed NMM, called Wilson and Covan model, comprised two units: a pyramidal neuron and an inhibitory interneuron population (Figure 1.3a) [13]. The model could produce a single activity on the alpha band 7.5–12.5 Hz).

In Figure 1.3b it can be observed the next step of the NMM development: the Jansen model. It consists of connecting, with a positive feedback, an excitatory interneuron population to the pyramidal population of the previous model. This permitted to generate delta ($1 - 4$ Hz) and theta ($4 - 7$ Hz) rhythms. This model was the first able to reproduce experimentally observed visual-evoked potentials [14].

A few years later, Wendling model was proposed. It was based on adding a population of fast inhibitory interneurons to the Jansen model (Figure 1.3c). This model was able to generate beta ($13 - 30$ Hz), and gamma ($30 - 150$ Hz) activity [15].

Another improvement consisted of adding a self-feedback to the inhibitory interneuron population of the Jansen model (Figure 1.3d). This self-feedback is realistic because it is present in real neurons systems, particularly in populations of fast GABA, which is an inhibitory neurotransmitter and the main generator of gamma band activity [16].

The first model capable of generating multiple-frequency components was Ursino's model [17]. It is based on adding a static self-feedback to the fast inhibitory interneurons of the Wendling model. This produces a self-inhibition, resulting in gamma oscillations when the neurons are excited with an extra noise source. The obtained gamma oscillation can coexist with the lower band activity, which is also driven by a source of independent noise fed to the pyramidal neurons, as we can see in Figure 1.3e.

Finally, Figure 1.3f represents the model in which we are going to focus through this master thesis. The model has two main features to differentiate from Ursino's model. First, a modulatory parameter introduced to the firing frequency of the fast inhibitory population, and then, a dynamic self-feedback on the same population (replacing the previous static self-feedback) [2].

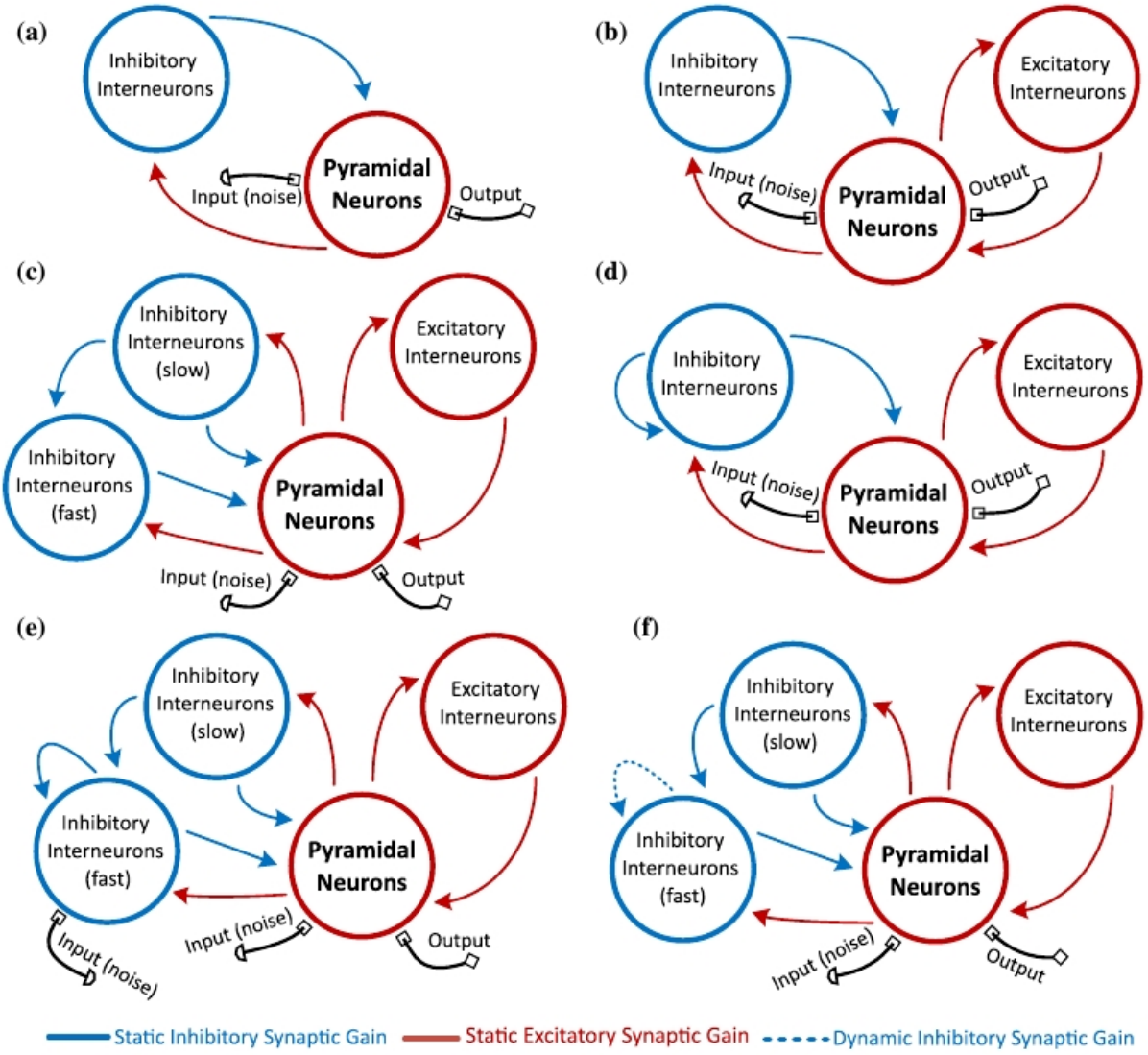

Figure 1.3. Evolution of neural mass models. From [2].

Outline

The goal of the present work is to study the usability of a neural mass model to model the synchronized brain oscillations.

The starting point is the presentation of several basic biological elements, whose understanding is fundamental to follow the scope of this work. This is follow by the explanation of the methodology employed to assess the synchronization in oscillations presenting different frequency bands: the cross-frequency coupling (CFC) and the cross-frequency directionality (CFD).

The next step will be to present two different NMMs. First, the one shown in Figure 1.3f [2]; and then, a version which connects multiple NMMs like the first model. Both NMMs are referred to as single node NMM, and multiple node NMM.

Then, we study if by changing the control parameters of the single node NMMs we can reproduce the experimental results of the scientists from the *Instituto de Neurociencias de Alicante* [1], whose main finding is that gamma oscillations modulate the theta rhythms in the hippocampus.

Finally, I represent a NMM comprised of two nodes from Ref. [3], and show the functionality of the NMM developed for multiple nodes .

Chapter 2

Theoretical Framework

2.1. Neurons and Synapses

A neuron is an electrically excitable cell that receives, processes, and transmits information through electrical and chemical signals. They are the primary components of the central nervous system, comprising the brain, spinal cord and peripheral nervous system.

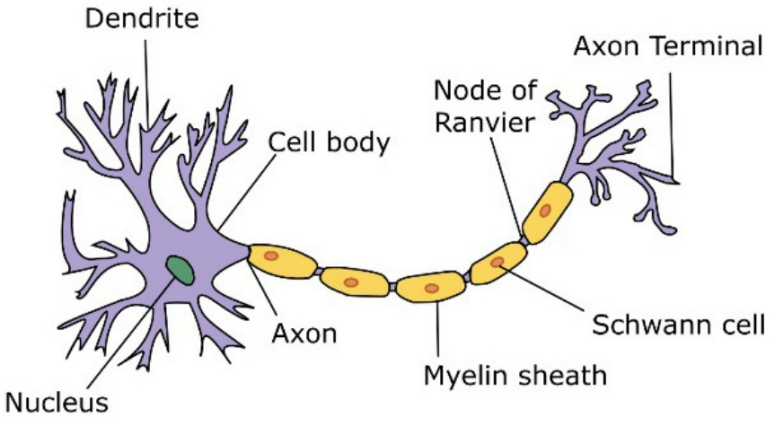

Figure 2.1. Anatomy of a neuron.

A typical neuron consists of a cell body (soma), which contains the nucleus; dendrites, which receive the input from presynaptic neurons; and an axon, which transports the electrical signal from the soma to the axon terminals (Figure 2.1). Along the axon, there are parts which are covered with Schwann cells, providing the myelin sheath that increase the speed at which the electrical signal travels. They act as a insulating material and achieve faster jumps of the action potential from gap to gap. These uncovered gaps are called nodes of Ranvier.

The behavior of the neuron membrane is comparable to a RC circuit, with characteristic differences of potential, currents, resistances, and capacitances. The electrical signal is the difference in the potential between the intracellular and the extracellular medium, called membrane potential. The currents correspond to the flux of ions, mainly Na^+, K^+ and Cl^-. In addition, membranes behave as parallel resistances to the membrane potential, hampering the charges to diffuse across the membrane. In addition, the membrane behaves as a set of parallel capacitors, since its both sides are polarized.

Under resting conditions, the inside of the cell is negatively charged with respect to the surrounding extracellular fluid. The membrane potential is about -70 mV, and the cell is said to be polarized.

Neurons transmit characteristic electrical pulses, called action potential or spikes, in response to chemical and electrical inputs. In Figure 2.2 we can observe the steps of an action potential.

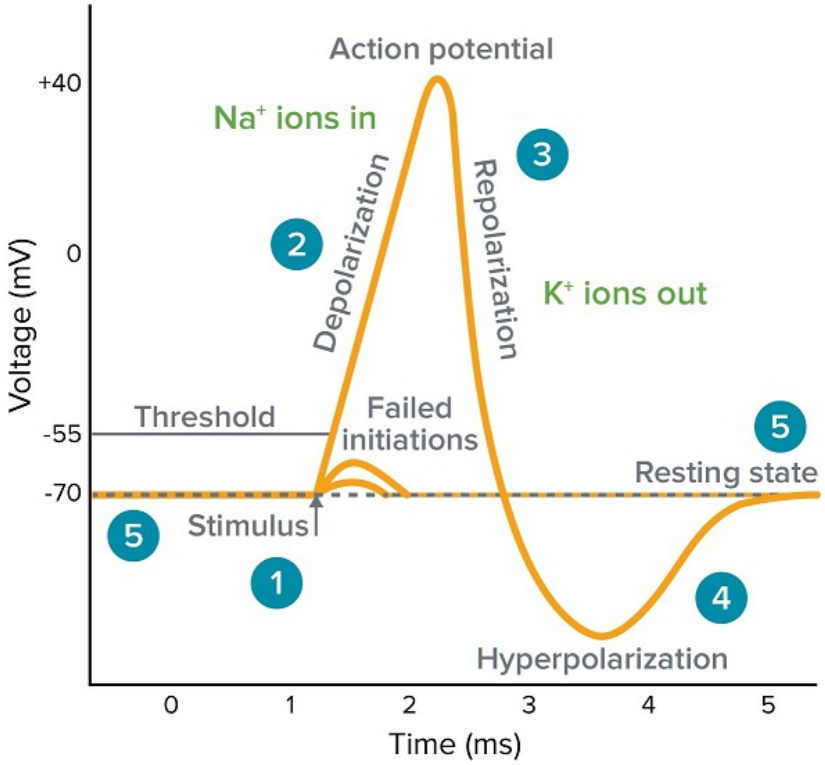

Figure 2.2. Dynamics of an action potential. (1) A stimulus rapidly increases the membrane potential. A threshold should be raised to start the membrane depolarization. (2) During depolarization, sodium channels open, leading to a large influx of sodium ions. (3) Rapidly, the sodium channel inactivates and there is a large efflux of potassium ions (resulting from activated potassium channels) These actions cause the membrane repolarization. (4) Aferwards,the membrane potential is lowered (hyperpolarization). This is caused by the efflux of potassium ions and the closing of the potassium channels. (5) The membrane potential returns to the resting state again. Printed from [18].

Despite the local effect of the action potential, the spike travels via the axon, starting in the dendrites and ending at the axon terminals, where spike is forwarded to other neurons via a synapse.

Synapses are the structures that permit a neuron to pass a signal to another neuron or to another target cell. The signal could be electrical (propagation through a small gap) or chemical (release of neurotransmitters), which are the most common in the brain. In terms of the kind of released neurotransmitters chemical synapses can be excitatory or inhibitory:

1. **Excitatory synapse**. The interaction of the neurotransmitters with the receptors of the postsynaptic neuron opens sodium (Na^+) and potassium (K^+) channels. The influx of sodium (from the external side to the postsynaptic neuron) is larger than the efflux of potassium, so the postsynaptic membrane is depolarized, generating an excitatory postsynaptic potential (EPSP).

2. **Inhibitory synapse**. The interaction of the neurotransmitters with the receptors of the postsynaptic neuron open potassium (K^+) and chloride (Cl^-) channels. The efflux of potassium and the influx of chloride cause the postsynaptic membrane to be hyperpolarized, generating an inhibitory postsynaptic potential (IPSP).

2.2. The Hippocampus

The hippocampus is part of the hippocampal formation, which is located in the temporal lobe. The hippocampal formation is a group of brain areas consisting of the dentate gyrus (DG), hippocampus, subiculum (Sub), presubiculum (Pre), parasubiculum (Para), and entorhinal cortex (EC). Particularly, the hippocampus has three subdivisions: CA3, CA2, and CA1. [19]

The information in the hippocampal circuit spreads mainly unidirectional. The entorhinal cortex is the first step, since it recibes much of the neocortical input reaching the hippocampal formation. Then, the second layer cells of the entorhinal cortex give rise to axons that project mainly to the dentate gyrus through the perforant path, which does not project back to the entorhinal cortex. Likewise, granule cells of the dentate gyrus give rise to axons connecting with the CA3 hippocampal field, which do not project back either. CA3 pyramidal cells, in turn, mainly project to the CA1 hippocampal field. Following the pattern, CA1 does not project back to CA3. CA1 projects unidirectionally to the subiculum, providing its major excitatory input (again, without projecting back). CA1 also projects axons to the entorhinal cortex. In turn, subiculum projects to the presubiculum and the parasubiculum, but its more predominant cortical projection is directed to the entorhinal cortex deep layers, closing the hippocampal processing loop. Figures 2.3 and 2.4 represent an overview of the hippocampal connection set.

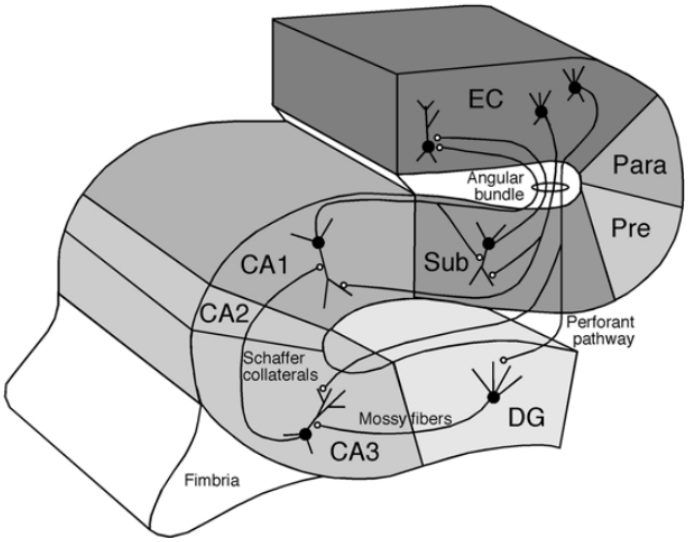

Figure 2.3. The hippocampal formation. Connections are pointed with solid black lines. Black (white) dots represent the starting(ending) point of each projection. Image from [19].

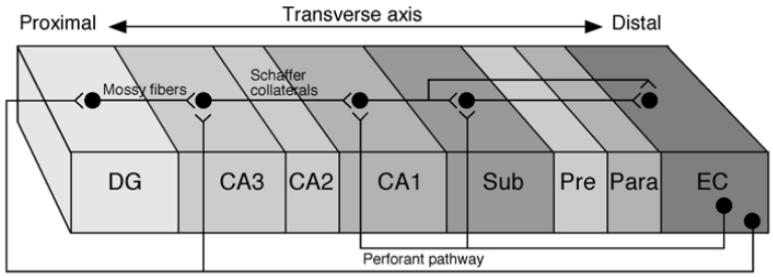

Figure 2.4. Projections along the transverse axis of the hippocampal forma- tion; the dentate gyrus is located proxi- mally and the entorhinal cortex distally. Image from [19].

Furthermore, the hippocampus belongs to the limbic system and it is important to consolidate information from short-term to long-term memory. It also plays a significant role in the spatial memory that enables navigation.

The hippocampus is one of the first areas of the brain to suffer damage in several brain diseases, such as Alzheimer's disease [20] or Schizophrenia [21].

2.3. Neural Oscillations

Neural oscillations, also known as brainwaves, are rhythmic or repetitive patterns of neural activity in the central nervous system. Generally, brainwaves can be characterized by their frequency, amplitude and phase. There are two main different neural oscillations, depending on whether the brainwave is caused by a single neuron or a neural ensemble.

At a single neuron level, oscillations can appear in the membrane potential, or as rhythmic patterns of action potentials, which then produce oscillatory activation of post-synaptic neurons.

On the other hand, interactions between groups of neurons can lead to a synchronized oscillatory activity, which generally arises from feedback connections between the neurons. This results in the synchronization of their firing patterns, which can produce macroscopic oscillations, and thus, observed in an electroencephalogram (EEG). The interaction between neurons can lead to oscillations at different frequencies than the firing frequency of individual neurons. The frequency bands of oscillatory activity in groups of neurons are the following: delta $(1-4$ Hz), theta $(4-7$ Hz), alpha $(7.5-12.5$ Hz), beta $(13-30$ Hz), and gamma $(30-150$ Hz) [22].

To understand the importance of group neural oscillations, we can highlight some aspects. For example, different sleep stages are featured by their spectral content, since EEG signals alter during sleep from faster frequencies to increasingly slower frequencies [23]. Also, neural oscillations have been linked to the emergence of coherent behaviour and cognition [24], consciousness [25], or even meditation [26]. Besides, focusing on hippocampus, theta-gamma uncoupling has been proposed as an early electrophysiological signature of hippocampal network impairment in Alzheimer's disease [27] or schizophrenia [28].

2.4. Cross Frequency Coupling (CFC)

The interactions between oscillations at different frequency bands are known as cross-frequency coupling (CFC). There are many synchronized neuronal assemblies in the brain, each of them supporting a frequency band of the network rhythm. By studying the relationship between these frequencies we can understand the interaction between local neural circuits, as well as observing its intrinsic properties.

There are six types of CFC of interest to electro-physiology: phase-phase, phase-frequency, phase-amplitude, frequency-frequency, amplitude-amplitude and amplitude-frequency couplings (PPC, PFC, PAC, FFC, AAC, and AFC, respectively) (Figure 2.5) [29]. Several empirical studies have observed PPC, PAC, and occasionally AAC. On the contrary, PFC, AFC and FFC have not been empirically observed [3].

One of the best-known example of this type of CFC occurs in the hippocampus. Some studies suggest that the theta oscillations (4–7 Hz) phase modulates the gamma oscillation [30–32]. But other recent studies have also shown that the amplitude of gamma oscillations modulates the phase of theta [1, 33]. Another example is the case of human neocortex, where the phase of the low-frequency theta rhythm modulates the power of the high gamma frequency (80 to 150 Hz) [34].

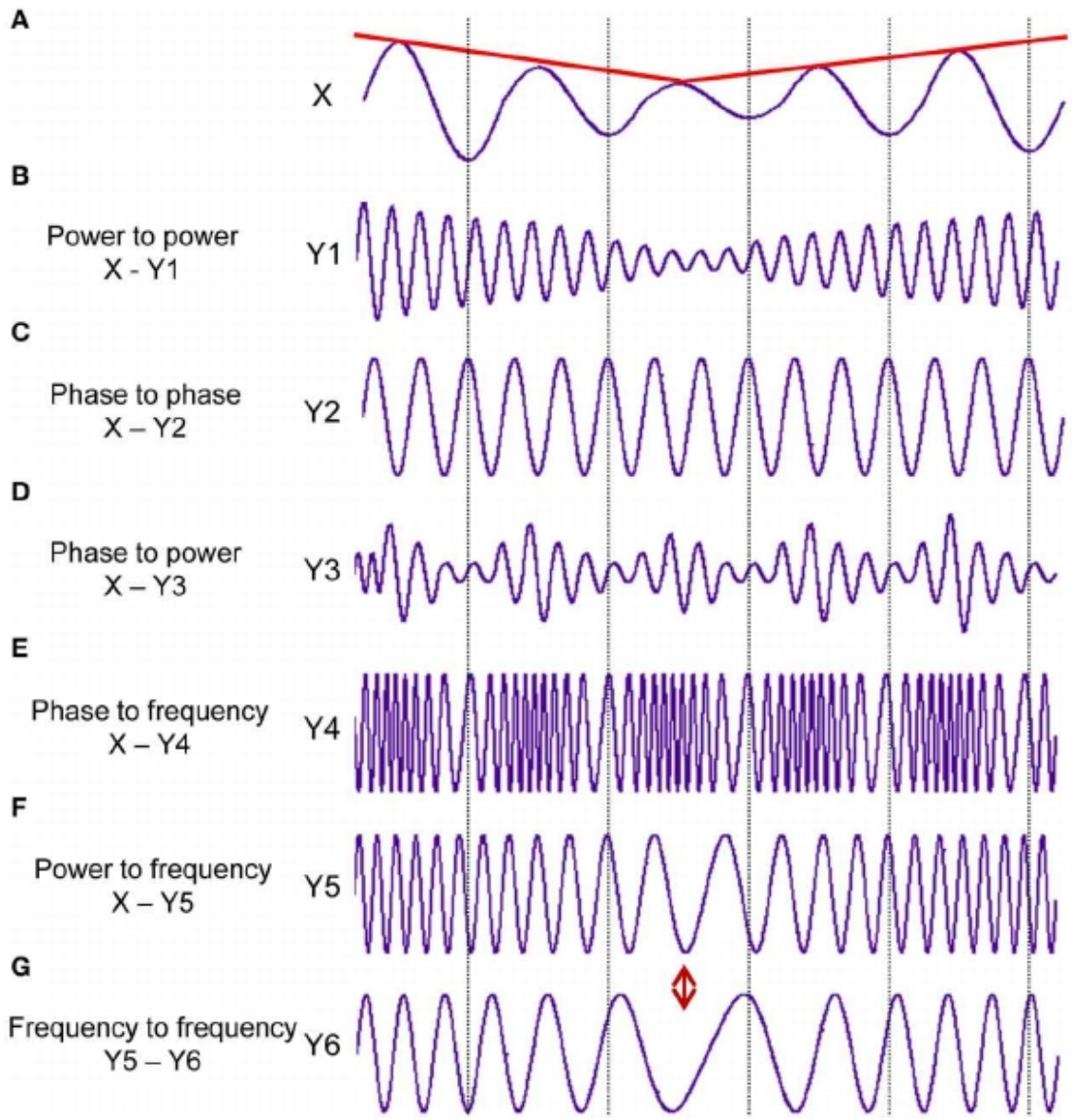

Figure 2.5. Different types of the cross-frequency coupling. (A) Signal X at a constant frequency with a fluctuating amplitude over time (red line). (B) AAC: Signal Y1 showing slow amplitude modulations over time like signal X (red line). (C) PPC: One oscillation period of signal X corresponds to three periods of signal Y2. (D) PAC: Fast amplitude modulations of signal Y3 are coupled with the phase of the signal X. (E) PFC: Frequency modulations of signal Y4 are coupled with phase changes of signal X. (F) AFC: Frequency modulations of signal Y5 are coupled with the slow amplitude modulations of signal X (red line). (G) FFC: Signal Y6 has slower frequency modulations than in signal Y5. Image from [35].

Particularly, in the present study, we are interested in assessing the phase-amplitude coupling (PAC). Normally, PAC is evaluated between two signals, at a certain pair of frequencies. One signal contains the phase modulatory component at a given frequency value, while the other one contains the amplitude-modulated component at a different frequency. Throughout this master thesis, we will mainly analyze local PAC, i.e., the same signal is the modulatory and modulated component.

In order to assess the PAC, I have used a Matlab code provided by Víctor López-Madrona [36]. The algorithm follows the method of Kullback-Leibler distance, a function that is used to infer the distance between two distributions, and calculates how much an empirical amplitude distribution-like function over phase bins deviates from the uniform distribution [37]. It also includes a statistical analysis based on block-resampling at single locations [34]. In Appendix A it is found a more in-depth explanation of the algorithm.

2.5. Cross Frequency Directionality (CFD)

It is also required to evaluate the directionality of the PAC, i.e., if the phase of the slower oscillations drives the amplitude of the faster oscillation, or vice versa. To do so, we use the cross-frequency directionality (CFD). This measure relies on the phase-slope index (PSI) between the phase of slower oscillations and the amplitude envelope of the faster oscillation [33].

Once more, I have employed Víctor López-Madrona's Matlab code to analyse the cross-frequency directionality (CFD) [36]. In Appendix A it is found a more in-depth explanation of the algorithm.

Chapter 3

The Neural Mass Model (NMM)

3.1. A NMM of 1 node

NMMs are neurologically inspired computational models of brain dynamics at the level of neural masses, i.e., populations of several thousands to several millions of neurons with similar characteristics [11]. NMMs are composed of units of a single type population neurons, each of which models the joint dynamics.

A single unit is shown again in Figure 3.1. The inputs to the unit are the unweighted postsynaptic potentials from other units $v_{u'}$, reflecting the mean excitatory postsynaptic potential (EPSP) or mean inhibitory postsynaptic potential (IPSP) for units representing excitatory or inhibitory populations, respectively. $I_{ue}(I_{ui})$ represents the set of excitatory (inhibitory) inputs of a unit u. Likewise, colored noise V_N is also considered. It represents the unmodeled dynamics of the neighboring cortical regions, as well as possible uncertainties. In this case, only pyramidal type units are excited by noise. Each input synaptic potential is weighted by a constant connectivity strength, $C_{uu'}$ (u accounts for the target and u' accounts for source population), called synaptic gains, which are proportional to the number of synaptic connections between the populations. Likewise, K_u represents the noise gain.

The weighted sum of inputs plus the noise is the mean membrane potential V_{Mu}, which is converted to the mean firing rate $\sigma_u(V_{Mu}(t))$ by means of the sigmoid function. The sigmoid confines the firing rate to the open interval $]0, \nu_{max}[$, where ν_{max} is the maximum mean firing rate. V_θ reflects the expected spiking threshold voltage of the individual neurons in the population. Also, r determines the slope of the sigmoid, and represents the inverse of the standard deviation of the firing thresholds.

In turn, the mean firing rate enters a second-order differential equation reflecting the evolution of the unweighted mean postsynaptic potential v_u. G_u represents the average dendritic gain of the population u; and ω_u^{-1} is the average time constant of the membrane potential of population u, which measures the velocity at which a neuron's voltage level decays to its resting state after it receives an input signal.

The dynamics of a single unit is defined with the following equations [2]:

$$V_{Mu}(t) = \sum_{u' \in I_{ue}} C_{uu'} v_{u'}(t) - \sum_{u' \in I_{ui}} C_{uu'} v_{u'}(t) + K_u V_N(t) \tag{3.1}$$

$$\sigma_u(V_{Mu}(t)) = \frac{2\nu_{max}}{1 + e^{-r\left(V_{Mu}(t) - V_\theta\right)}} \tag{3.2}$$

$$\frac{\mathrm{d}^2 v_u}{\mathrm{d}t^2} = G_u \omega_u \sigma_u \left(V_{Mu}\left(t\right)\right) - 2\omega_u \frac{\mathrm{d}v_u}{\mathrm{d}t} - \omega_u^2 v_u\left(t\right) \tag{3.3}$$

The Laplacian transform of the differential equation 3.3 is equivalent to the dendritic transfer function given in Figure 3.1.

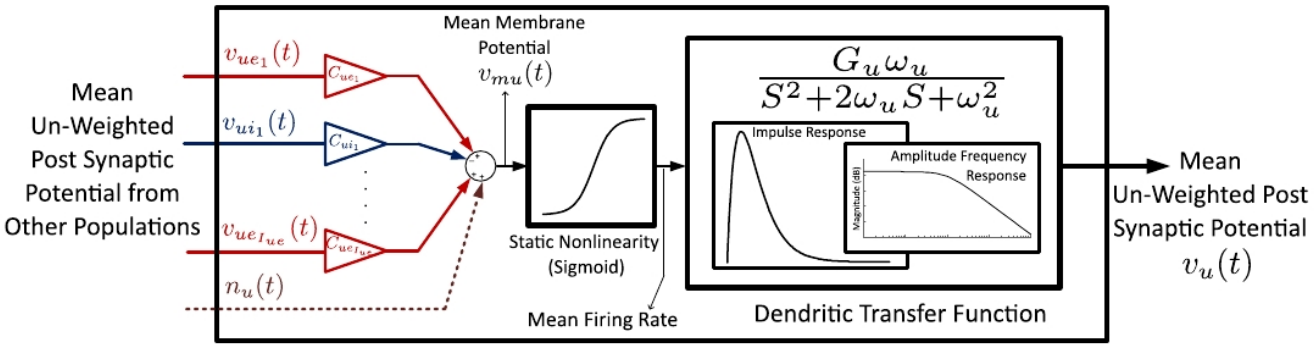

Figure 3.1. Single neural mass unit. $v_{ue_1}(v_{ui_1})$ is an example of an unweighted mean presynaptic potential, or postsynaptic potential from other units, of the $ue_1(ui_1)$ excitatory (inhibitory) population, which unit u has as input. $I_{ue}(I_{ui})$ is total number of excitatory (inhibitory) input units. n_u represents the colored noise. The mean membrane potential, represented with v_{mu}, is obtained by weighted summation of the mean presynaptic potentials. The sigmoid function represents the correspondence between the mean membrane potential and the mean firing rate. The 2nd order differential equation 3.3 is the Laplacian representation of the dendritic transfer function. The insets provide the impulse response and amplitude–frequency response of the dendritic transfer function. Figure from [2].

The mean membrane potential of the pyramidal neuron unit is the output of the NMM, which represents a mesoscopic recording of the brain activity.

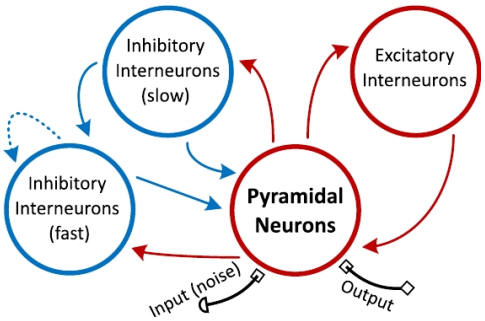

Figure 3.2. NMM proposed in [2]. Blue solid lines represents a static inhibitory synaptic gain, blue dashed lines represents a dynamic inhibitory synaptic gain, and red line represents a static excitatory synaptic gain. Figure adapted from [2].

The four different neuron populations which have been considered in this model are pyramidal neurons (p), excitatory interneurons (q), slow inhibitory interneurons (s) and fast inhibitory interneurons (f).

Generally, pyramidal neurons present a larger somatic diameter and an irregular shape, as compared with interneurons that have a smaller and more rounded soma. Pyramidal neurons are also excitatory neurons, but slower that the excitatory interneurons. Excitatory and inhibitory interneurons tend to generate EPSPs and IPSPs, respectively. Specifically, inhibitory interneurons play an important role in producing neural ensemble synchrony by generating a narrow window for effective excitation and rhythmically modulating the firing rate of the excitatory neurons [38]. In the presented model, the slow inhibitory population is the main source of alpha band activity, whereas the fast inhibitory population serves as the source of gamma band activity [2].

As one can observe in Figure 3.2, the pyramidal neuron population unit excites the other interneuron population units. In turn, it receives input from them, as well as a driving input or colored noise, which represent the average firing rate of neighboring regions not included in the model. Moreover, the slow inhibitory interneuron population unit inhibits the fast inhibitory interneuron population unit.

The fast inhibitory interneuron population has an extra state variable, $v_{ff}(t)$, for the dynamic self-inhibition. It serves as a low pass filter with cut-off frequency $f_c = \frac{1}{2\pi\tau_f}$, i.e., self-inhibition or self-synaptic gain is weak for larger frequencies than f_c.

The parameter P_f accounts for the integration of the mean excitatory influence from other regions on the mean firing rate of the fast inhibitory unit, i.e., represents the influence of an excitatory input to the fast inhibitory interneuron population. Particularly, increasing the value of P_f reduces the mean threshold membrane potential of the fast inhibitory population and the mean membrane potential of the pyramidal population V_{mp}.

The effect generated by P_f and the self-inhibition feedback causes the fast inhibitory population to operate as a source of fast oscillatory activity, producing a limit-cycle behavior in the frequency range of the slow and fast bands.

Colored noise is generated by passing Gaussian noise (mean ν_p and variance σ_p^2) through the excitatory dendritic transfer function of the pyramidal neurons, to convert it to a voltage. Furthermore, it is important to notice that the sigmoid function is the seed for the model nonlinearities.

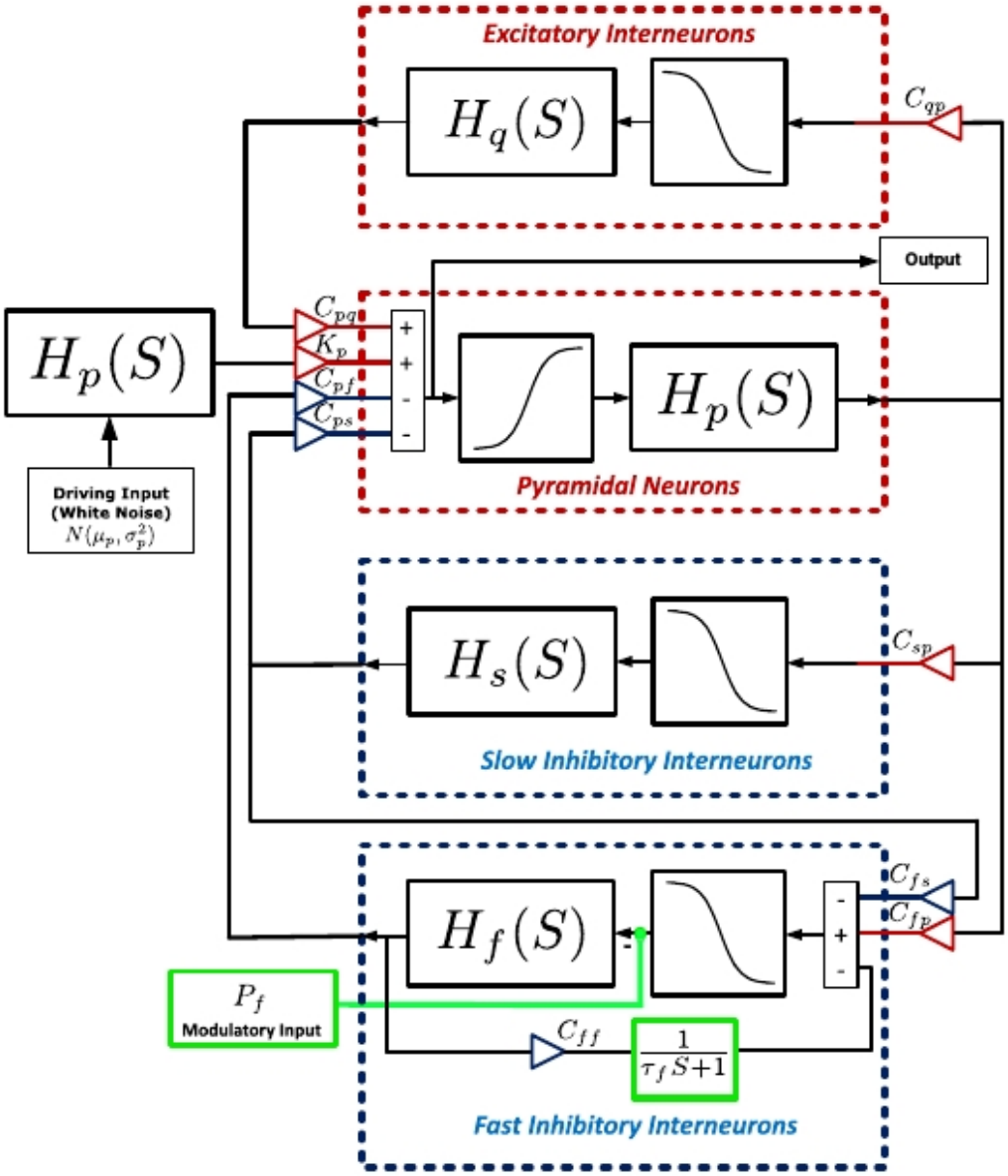

Figure 3.3. Conections between populations in the proposed NMM [2]. The excitatory (inhibitory) populations are in dashed red (blue) boxes. In green one can observe the modulatory parameter P_f and the first-order dynamics in the self-feedback of the fast inhibitory unit. Figure taken from [2].

One can observe a more exhaustive representation of the model in Figure 3.3. The dynamics of the model is described with the following equations:

- **Pyramidal neurons**

$$V_{Mp}(t) = C_{pq}v_q(t) - C_{ps}v_s(t) - C_{pf}v_f(t) + K_pV_N \tag{3.4}$$

$$\sigma_p(V_{Mp}(t)) = \frac{\nu_{max}}{1 + e^{-r\left(V_{Mp}(t) - V_\theta\right)}} \tag{3.5}$$

$$\frac{\mathrm{d}^2v_p}{\mathrm{d}t^2} = G_p\omega_p\sigma_p\left(V_{Mp}\left(t\right)\right) - 2\omega_p\frac{\mathrm{d}v_p}{\mathrm{d}t} - \omega_p^2v_p\left(t\right) \tag{3.6}$$

- **Excitatory Interneurons**

$$V_{Mq}(t) = C_{qp}v_p(t) \tag{3.7}$$

$$\sigma_q(V_{Mq}(t)) = \frac{\nu_{max}}{1 + e^{-r\left(V_{Mq}(t) - V_\theta\right)}} \tag{3.8}$$

$$\frac{\mathrm{d}^2v_q}{\mathrm{d}t^2} = G_q\omega_q\sigma_q\left(V_{Mq}\left(t\right)\right) - 2\omega_q\frac{\mathrm{d}v_q}{\mathrm{d}t} - \omega_q^2v_q\left(t\right) \tag{3.9}$$

- **Slow Inhibitory Interneurons**

$$V_{Ms}(t) = C_{sp}v_p(t) \tag{3.10}$$

$$\sigma_s(V_{Ms}(t)) = \frac{\nu_{max}}{1 + e^{-r\left(V_{Ms}(t) - V_\theta\right)}} \tag{3.11}$$

$$\frac{\mathrm{d}^2v_s}{\mathrm{d}t^2} = G_s\omega_s\sigma_s\left(V_{Ms}\left(t\right)\right) - 2\omega_s\frac{\mathrm{d}v_s}{\mathrm{d}t} - \omega_s^2v_s\left(t\right) \tag{3.12}$$

- **Fast Inhibitory Interneurons**

$$\tau_f\frac{\mathrm{d}v_{ff}}{\mathrm{d}t} = -v_{ff}(t) + v_f(t) \tag{3.13}$$

$$V_{Mf}(t) = C_{fp}v_p(t) - C_{fs}(t)v_s(t) - C_{ff}v_{ff}(t) \tag{3.14}$$

$$\sigma_f(V_{Mf}(t)) = \frac{\nu_{max}}{1 + e^{-r\left(V_{Mf}(t) - V_\theta\right)}} - P_f \tag{3.15}$$

$$\frac{\mathrm{d}^2v_f}{\mathrm{d}t^2} = G_f\omega_f\sigma_f\left(V_{Mf}\left(t\right)\right) - 2\omega_f\frac{\mathrm{d}v_f}{\mathrm{d}t} - \omega_f^2v_f\left(t\right) \tag{3.16}$$

- **Colored noise (model input)**

$$n_p(t) = N(\mu_p, \sigma_p^2) \tag{3.17}$$

$$\frac{\mathrm{d}^2V_N}{\mathrm{d}t^2} = G_p\omega_pn_p(t) - 2\omega_p\frac{\mathrm{d}V_N}{\mathrm{d}t} - \omega_p^2V_N\left(t\right) \tag{3.18}$$

There are several advantages of the proposed NMM. First, it can produce multiple frequency components with parameters in the biophysiologically plausible range [15]. In addition, fast activity can be tuned without shifting the features of the default alpha band activity. Also, since there is a single source of noise, the activity bands present a stronger phase-amplitude correlation.

3.2. A NMM with N nodes

In this section, I present a proposal for a neural mass model of a specific number of nodes. This model has been built on the basis of an existing neural mass model for two nodes [3].

All the previously variables and parameters used in the single node NMM from Section 3.1 are also used in this model. Nevertheless, there are several important differences between both of them, which will be explained hereunder.

First, we want to highlight that sub index α is used for differentiating between nodes. Thus, many of the parameters used in this model are the same as in the single node case adding the sub index α. Additionally, u still accounts for the neuron population, as in the previous model. The neural populations units are also the same as in the single node case. Table 3.1 shows the connections between populations.

Table 3.1. Excitatory and inhibitory connections between populations in the multiple nodes NMM. Note that the subindex for each contribution is pointed.

Population	I_{ue}	I_{ui}
Pyramidal (p)	Excitatory (q)	Slow inhibitory (s), Fast inhibitory (f)
Excitatory (q)	Pyramidal (p)	-
Slow inhibitory (s)	Pyramidal (p)	-
Fast inhibitory (f)	Pyramidal (p)	Slow inhibitory (s), Self-inhibition (ff)

;

Another important difference to be pointed out is that the previously used modulatory parameter P_f in the fast inhibitory interneurons sigmoid function, is replaced by a noise component on the mean membrane potential of the same population ($K_{\alpha f}V_{N\alpha}$). Therefore, we use the same sigmoid function for all the different populations. In addition, an interesting feature of this model is that by tuning the mean input noise level of each node (P_α), we can obtain five out of the theoretically proposed six different coupling types which has been presented in Section 2.4.

The dynamics of a single node in a NMM of a certain number of nodes could be described as follows:

Equations for a given node α

1. General equations for each of the four populations:
   (16 equations)

   a) **Mean firing rate**:

$$\sigma(V_{M\alpha u}(t)) = \frac{\nu_{max}}{1 + e^{-r\left(V_{M\alpha u}(t) - V_\theta\right)}} \tag{3.19}$$

   b) **Mean membrane potential**:

$$V_{M\alpha u}(t) = \underbrace{\sum_{u' \in I_{ue}} C_{\alpha u u'} v_{\alpha u'}(t)}_{Excitatory\ inputs} - \underbrace{\sum_{u' \in I_{ui}} C_{\alpha u u'} v_{\alpha u'}(t)}_{Inhibitory\ inputs} + \underbrace{K_{\alpha u} V_{N\alpha}(t)}_{Input\ noise} + \underbrace{\sum_{\beta \in I_\alpha} K_{\alpha\beta} v_{\alpha\beta u}(t)}_{Input\ between\ nodes} \tag{3.20}$$

   c) **Mean post synaptic potential**:

$$\frac{\mathrm{d}^2 v_{\alpha u}}{\mathrm{d}t^2} = G_{\alpha u}\omega_{\alpha u}\sigma\left(V_{M\alpha u}(t)\right) - 2\omega_{\alpha u}\frac{\mathrm{d}v_{\alpha u}}{\mathrm{d}t} - \omega_{\alpha u}^2 v_{\alpha u}(t) \tag{3.21}$$

2. **General equations for the external inputs from the other nodes**:
   ($N-1$ equations, being N the total number of nodes)

$$\frac{\mathrm{d}^2 v_{\alpha\beta u}}{\mathrm{d}t^2} = G_{\alpha\beta u}\omega_{\alpha\beta u}\sigma\left(V_{M\beta u}\left(t\right)\right) - 2\omega_{\alpha\beta u}\frac{\mathrm{d}v_{\alpha\beta u}}{\mathrm{d}t} - \omega_{\alpha\beta u}^2 v_{\alpha\beta u}\left(t\right) \tag{3.22}$$

   (u relates to the type of population which connects each pair of nodes)

3. Rest of equations:
   (3 equations)

   a) **Self-inhibition of the fast inhibitory interneuron population**:

$$\tau_{\alpha f}\frac{\mathrm{d}v_{\alpha ff}}{\mathrm{d}t} = -v_{\alpha ff}(t) + v_{\alpha f}(t) \tag{3.23}$$

   b) **External input as filtered noise**:

$$\frac{\mathrm{d}^2 V_{N\alpha}}{\mathrm{d}t^2} = G_{\alpha n}\omega_{\alpha n}n_\alpha\left(t\right) - 2\omega_{\alpha n}\frac{\mathrm{d}V_{N\alpha}}{\mathrm{d}t} - \omega_{\alpha n}^2 V_{N\alpha}\left(t\right) \tag{3.24}$$

   c) **White noise**:

$$n_\alpha(t) = N(P_\alpha, \sigma_\alpha^2) \tag{3.25}$$

Following with the differences between models, equation 3.20 requires a further explanation. The noise contribution (colored noise $V_{N\alpha}$) is different for each node, since the mean input noise level P_α can be tuned. The noise excitation weight $K_{\alpha u}$ can also differ depending on the population and the node.

Regarding the input between nodes, I_α represents the set of the nodes which have an information flow to node α. The parameter $K_{\alpha\beta}$ accounts for the synaptic gain from node β (source) to node α (target). The variable $v_{\alpha\beta u}$ represents the input of the mean post synaptic potential coming from node β to node α. The sub index u here reflects the type of population connecting the two nodes. The link between nodes employed in this model is the pyramidal neuron population.

Concerning equation 3.22, we compute the mean firing rate of the mean membrane potential of the node β, in order to include node β influence. Obviously, there are as many equations of this type for modeling one node, as the other nodes which provide an input to it.

It is also necessary to give the value of the average dendritic gain between node populations ($G_{\alpha\beta u}$) and the average time constant of the membrane potential between nodes α and β from u population (${\omega_{\alpha\beta n}}^{-1}$), which can be differently tune for different nodes connections. We remark that the reason why the two previous parameters are characterized with the sub index u is to permit that the connection between nodes occurs via any type of neuron population.

Regarding the external input as filtered noise (equation 3.24), the average dendritic gains of the filtered noise ($G_{\alpha n}$) and the average time constant of the filtered noise (${\omega_{\alpha n}}^{-1}$) can be modulated, in contrast to the single node NMM, in which the value of these parameters are fixed to G_p and ω_p^{-1}.

To facilitate the comprehension of the parameters, the list of their interpretation for a given node fixed parameters of the model are shown in Appendix B (Tables B.1 and B.2).

3.3. Application to the study of hippocampus

As we have seen, the neuron oscillations are a key reference signals for information processing in neuronal ensembles.

Particularly, a recent empirical study has observed the firing frequency of different areas in the hippocampus. This study consists in carrying out patchclamp recordings from mature hippocampal granule cells in vivo in the dentate gyrus of anesthetized and awake rats [39]. It shows two different coherences between postsynaptic currents and the local field potential (LFP) from the hippocampal granule cells. First, the inhibitory postsynaptic currents (IPSCs) generated by the interneurons, which showed coherence mainly in the gamma range (Figure 3.4, left). Then, the excitatory postsynaptic currents (EPSCs) generated by the entorhinal cortex, whose coherence was principally in the theta frequency band (Figure 3.4, right).

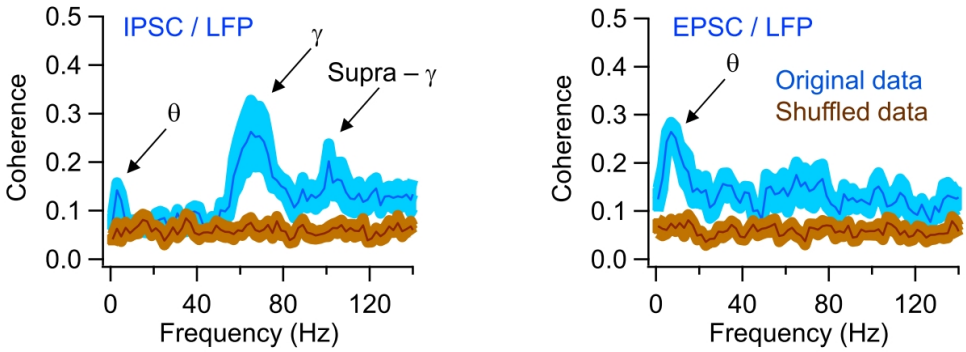

Figure 3.4. On the left (right), representation of the average coherence between IPSCs (EPSCs) and LFP of granule cells. Figure from [39].

Nevertheless, the main study in which we want to focus the attention is the last one carried out by scientists from the group of Santiago Canals from the Instituto de Neurociencias de Alicante. After having analyzed multiple theta and gamma activities in several hippocampal layers, they found that theta-gamma CFC is stronger between oscillations originated in the same hippocampal layer. Yet more interesting was that the CFD analysis pointed out that the amplitude of gamma oscillations sets the phase of theta rhythm in all layer-specific theta-gamma pairs, as can be seen in Figure 3.5. This result is contrary to the extended assumption, since the the majority of previous studies suggest that the fast oscillation amplitude is modulated by the phase of the slow one [30–32].

Throughout this master thesis I will try to reproduce using the neural mass models presented in Sections 3.1 and 3.2 the following facts:

- Modulate the position of the peak frequencies produced by the model to be located in the relevant frequency-bands of the experimentally recorded data.
- Assure the phase-amplitude coupling of the system (PAC) and seek of a cross-frequency directionality (CFD) that explain the finding that the amplitude of gamma oscillations sets the phase of theta in the hippocampus.

The procedure will consist on tuning several of the fitting parameters of the models, and then, analyze the qualitative differences with the model using the default parameters.

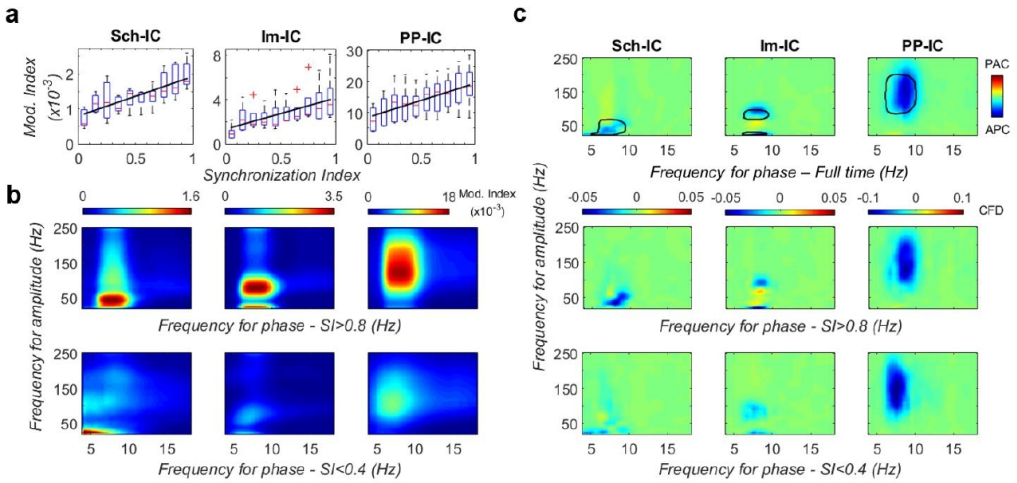

Figure 3.5. We focus on (b) and (c). Sch-IC, Im-IC and PP-IC corresponds to the stimulated pathways of the hippocampus. (b) represents the average CFC during epochs of high (upper) or low (lower) synchronization. (c) represents the within-layer CFD analysis. The pairs of theta-gamma oscillations with the highest CFC (encircled area) present the maximum negative values. Negative values implies that the phase of the slow oscillation modulates the amplitude of the fast. Figure from [1].

Chapter 4

Results and Discussion

In this Chapter, I reproduced the results of the the single node NMM presented in the previous chapter. Later, I present the results of tunning several control parameters of the model to test the possibility to modulate the position of the peak of the frequencies, and analyze the changes on the PAC and CFD.

As previously highlighted in Chapter 3.3, the theta-gamma PAC is stronger between oscillations originated in the same hippocampal layer. This is the reason why we are going to focus mainly on the analysis of a single node NMM.

Finally, I also reproduce the results of a NMM consisting in two nodes, in order to study the usability of the model, by varying the synaptic gains between the two nodes, and analyze the CFD and PAC. Apart from that, I show that the model can be potentially used for 3 nodes.

4.1. A NMM with 1 node

In Table 4.1 (Appendix B) we include the default values of the parameters used in the model. The majority of the parameters have been chosen in order to be in the biophysiologically plausible range proposed in Wendling model [15]. In addition, the parameters related to the noise (ν_p, σ_p^2, and K_p) have been selected in such a way that the three populations structure of the model, when uncoupled from the fast inhibitory population, operates in the alpha band region of activity [40].

The model has been simulated in Python 3, using a fourth order Runge-Kutta method. The time step value is fixed and corresponds to 0.001 seconds. Simulations for each case have been carried out for 242 seconds (unless otherwise specified), removing the first two seconds to avoid transient dynamics.

The power spectral density (PSD) is used to measure the relation of the power content of the voltage signals at a given frequency. In PSD representations, the power is plotted as $10log_{10}(P_{xx})$.

In order to test the computational implementation of the model, we represent in Figure 4.1 the membrane voltage of the pyramidal population, accompanied by the weighted postsynaptic potentials of the three interneuron populations obtained with the model. It can be observed that the excitatory interneuron population is in the saturation regime. Meanwhile, the fast inhibitory interneuron population generates fast activity due to the self-feedback dynamics.

The results in Figure 4.1 are not sufficient to assure the reliability of our model. Therefore, to ensure that the model is well represented, we also test if there is an anti-phase synchronization between the envelope of the fast inhibitory and slow inhibitory interneurons activity, which is the origin of the in-phase alpha–gamma PAC at the mean membrane potential of the pyramidal population. In Figure 4.2 is shown that we obtain a correct result.

Apart from that, the employed neural mass model has been compared with other models. First, a model of a single pyramidal population without any connection, and also, with a model composed by a pyramidal population and a inhibitory interneuron, as in the case of the Wilson and Covan model. In order to do so, Figure 4.3 represents the PSD of the three cases. As one can see, no frequency peak

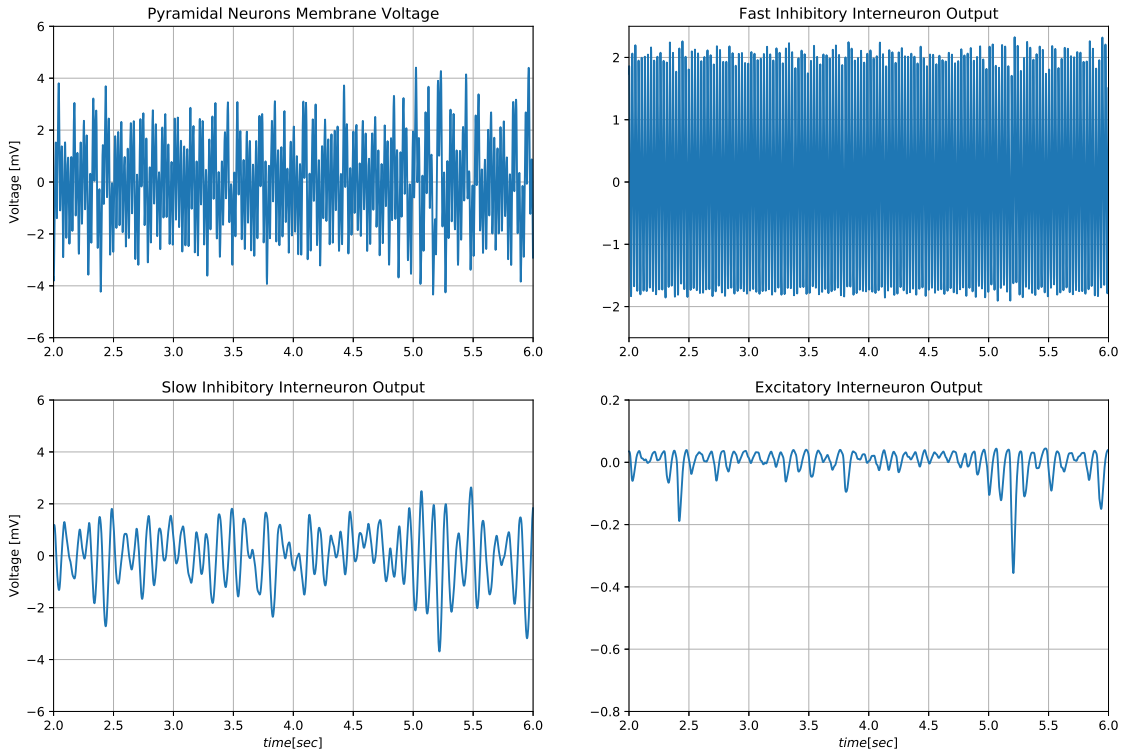

Figure 4.1. Dynamics of the membrane voltage of the pyramidal population and weighted postsynaptic potentials of the three interneuron populations. Simulations have been performed for 6 seconds, removing the 2 initial seconds to avoid the transient dynamics. Also, the signals have been normalized to a zero mean. Results represented from [2].

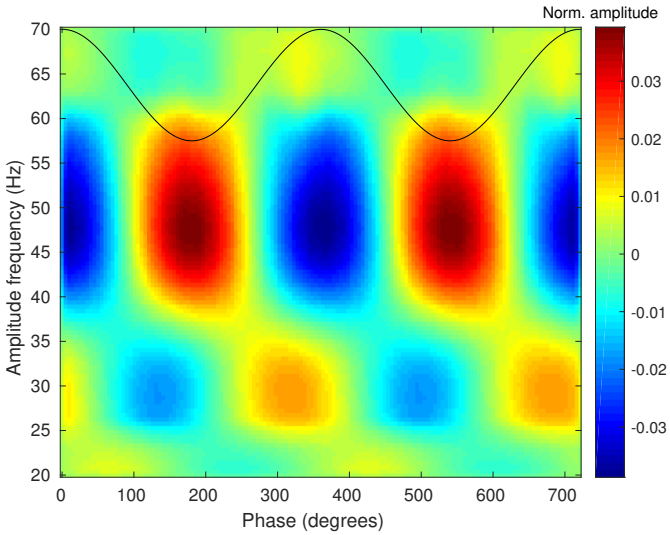

Figure 4.2. Representation of the power of the amplitude of the fast inhibitory population versus the phase of the slow inhibitory population postsynaptic potentials. One can observe that they are in anti-phase (the peak of the slow rhythm coincides with the minimum of the fast oscillation).

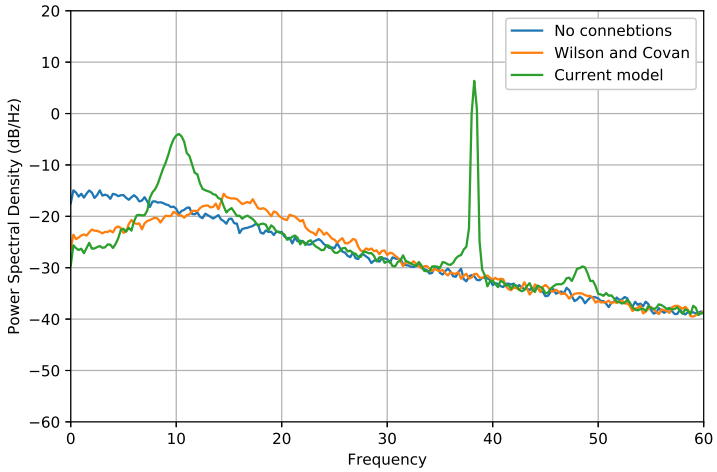

Figure 4.3. Representation of the power spectral density (PSD) of the membrane voltage of the pyramidal population (output of the neural mass model) for 3 different cases: (1) all the synaptic gains tuned to zero, thus the pyramidal population has no connections; (2) the pyramidal unit is only connected to the fast inhibitory population with the default values of synaptic gains C_{fp} and C_{pf}, imitating the Wilson and Covan model; and (3) using the default parameters of the model.

is generated with the first model. Conversely, the Wilson and Covan model allows us to generate a single peak in the beta band, as expected [13].

In Figure 4.4, the PSD of the membrane voltage of the pyramidal population and the weighted postsynaptic potentials of the three interneuron populations is represented. It can be observed that the model allows us to generate oscillations mainly in two frequencies: at roughly 10 Hz, in the alpha band; and at approximately 38 Hz, in the gamma band.

Having the prerequisite of activity in two frequency bands, we can focus on the study of the two issues presented at the end of Section 3.3. First, whether it is possible to modulate the position of the peaks of the frequencies by tuning any of the parameters. This could permit to fit the model to experimentally recorded data. Secondly, the response of the PAC and CFD to the variation of the parameters, with the particularity of trying to find a cross-frequency directionality from the amplitude gamma oscillations to the phase of theta activity.

4.1.1. Modulating the position of the frequency peaks

In this subsection, it is studied the response of the model to the variation of some of the fitting parameters. The parameters which have been selected are C_{fp}, C_{fs}, C_{pf}, ω_p, ω_s, ω_f and τ_f. C_{fp} and C_{pf} are selected because of their importance in the connection between the pyramidal and the fast inhibitory population for the phase-amplitude coupling. Furthermore, ω_p and ω_s are interesting candidates to modulate the peak of the slow frequency, since the circuit formed by the pyramidal and the slow inhibitory population is the main source of slow oscillations [2]. Moreover, since the fast inhibitory population with dynamic feedback is the source of fast oscillations, it is reasonable to assume that τ_f and ω_f are potential candidates to modulate the position of the high-frequency peak.

Regarding the synaptic gain from pyramidal to fast inhibitory interneurons unit C_{fp}, we find that changes in its value leaves unchanged the position of the low-frequency peak, as can be seen in Figure 4.5. This result disagrees with that presented in Ref. [2]. The biologically plausible explanation for our result is that changes in C_{fp} have a little influence on the circuit of the pyramidal and slow inhibitory populations, which is the main source of slow oscillations. When decreasing C_{fp} with respect to its reference value 0.3, the position of the high-frequency peak slightly rises, but diminishes its power. If we continue decreasing until $C_{fp} = 0$ the multiple-frequency peaks are maintained (not shown). This is because removing C_{fp} still permits the connection between the pyramidal to the fast

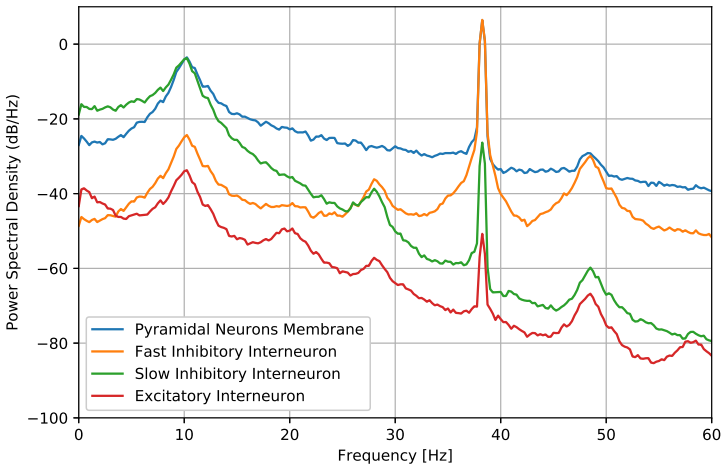

Figure 4.4. Representation of the power spectral density (PSD) of the membrane voltage of the pyramidal population (output) and the weighted postsynaptic potentials of the three interneuron populations. In the case of the output, one can observe the two peaks, at the alpha and gamma band respectively. This is also appreciable in both inhibitory interneurons. Additionally, it is remarkable that the slow inhibitory population is the main source of alpha activity; whereas the fast inhibitory, the main for fast activity. Represented from [2].

inhibitory population, through the slow inhibitory unit.

On the other hand, when increasing C_{fp} with respect to its reference value, the fast frequency peak shifts to smaller frequency values, as expected. Besides, there is a drop in the amplitude of the low-frequency peak. If the value of C_{fp} is increased further, the first peak disappears losing the multi-frequency feature (not shown). An explanation to account for this particular behavior is that by enhancing the communication between the pyramidal and the fast inhibitory population, the influence of the other units reduces, converting their synaptic gains to the pyramidal population in almost negligible. In order to generate the slow frequency band it is required the joint action of pyramidal and slow inhibitory population, so if the synaptic gains of these units are small compared to C_{fp}, the slow oscillations tend to fade away.

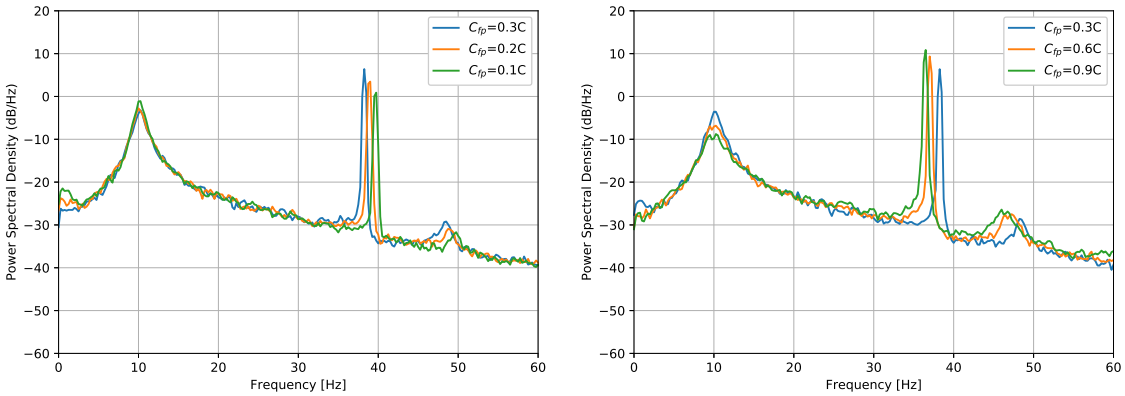

Figure 4.5. PSD comparison of the output of the model for different values of C_{fp}. Simulations performed for 240 seconds. On the left (right), the value of C_{fp} is slightly decreased (increased) with respect to the reference value $C_{fp} = 0.3C$.

In relation to the synaptic gain from fast inhibitory to slow inhibitory interneurons C_{fs}, Figure 4.6 shows that decreasing the value of C_{fs} barely influences the output of the model. The reason is that no matters if C_{fs} is small, the slow inhibitory population will have an influence on the pyramidal population through the synaptic gain C_{ps}.

Conversely, increasing C_{fs} leaves unchanged the position of the first peak of the PSD of the pyramidal membrane potential, but it reduces the power of the second one. Particularly, a value over two-fold of the default value washes out the fast-frequency peak. This is due to the influence of the oscillatory activity from the slow to the fast inhibitory population. These two oscillations are coupled at the input of the sigmoid nonlinearity of the fast inhibitory population. Thus, if C_{fs} is increased, the alpha activity of the fast inhibitory unit is enhanced (recall that the slow inhibitory population is the main source of alpha activity). This implies a depletion of the fast-frequency on the fast inhibitory unit, which will, in turn, alter the fast frequency of the pyramidal population.

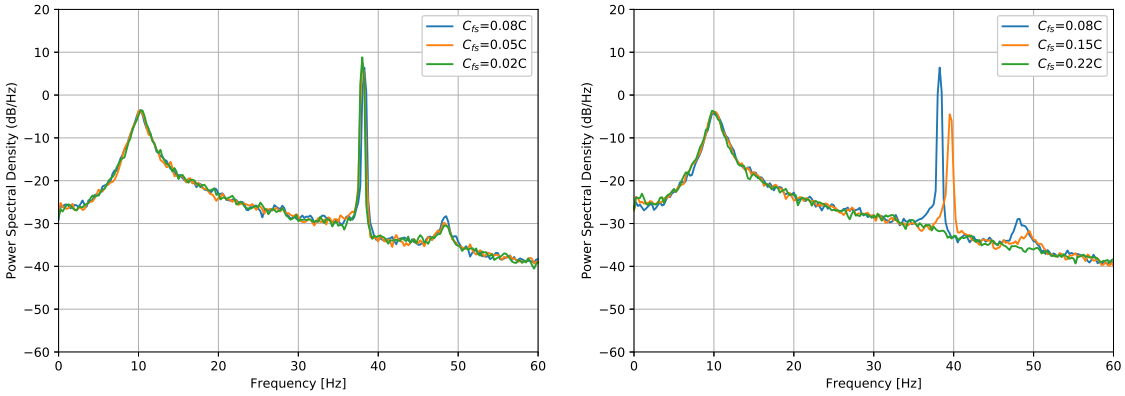

Figure 4.6. PSD comparison of the output of the model for different values of C_{fs}. Simulations performed for 240 seconds. On the left (right), the value of C_{fs} is slightly decreased (increased) with respect to the reference value $C_{fs} = 0.08C$.

By decreasing the synaptic gain from the fast inhibitory to pyramidal population C_{pf}, the modulation on the amplitude of the pyramidal unit coming from the fast activity is weaker, vanishing for $C_{pf} = 0$, as one can see in Figure 4.7. This is expected because C_{pf} is the unique synaptic gain connecting the source of fast oscillations (fast inhibitory unit) with the pyramidal unit.

Conversely, larger values of C_{pf} enhance the fast inhibitory activity, increasing the amplitude of the fast-oscillation and mitigating the slow activity. When increasing C_{pf} further, the slow-oscillations will eventually disappear due to the same reasons stated in the case of C_{fp}.

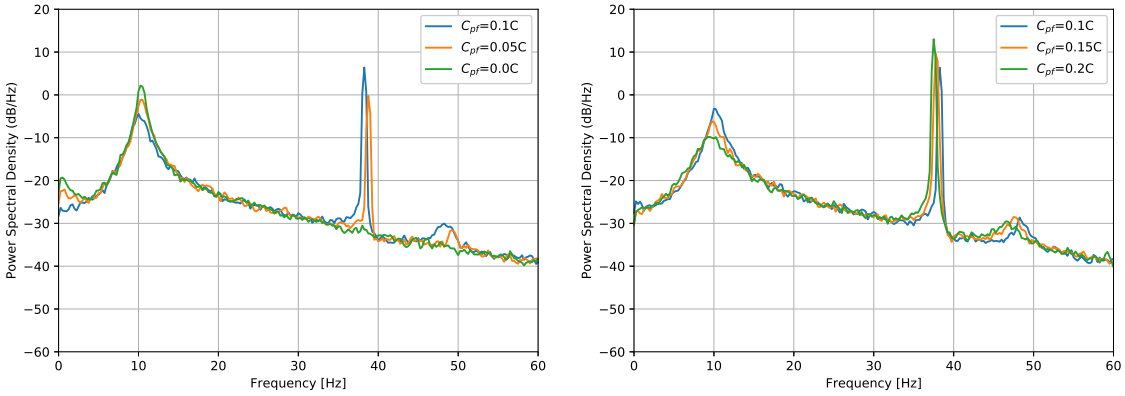

Figure 4.7. PSD comparison of the output of the model for different values of C_{pf}. Simulations performed for 240 seconds. On the left (right), the value of C_{pf} is slightly decreased (increased) with respect to the reference value $C_{pf} = 0.1C$.

In Figure 4.8, it can be seen that tuning the time constant of the pyramidal population ω_p leaves practically unchanged the position of the fast-frequency peak. Apart from that, by decreasing ω_p we can increase the power of the slow-frequency peak. However, decreasing ω_p also implies the formation of more peaks in different frequencies, which are the harmonics of the main frequencies. On the other hand, increasing ω_p reduces the power of the first peak. In the case of keep increasing ω_p the slow-oscillations will eventually disappear, and thus, lose the multi-frequency which characterizes the model. This is biologically plausible, since a higher ω_p entails a lower time at which the voltage level of neurons decays to its resting state after receiving a signal, promoting the generation of faster action potentials.

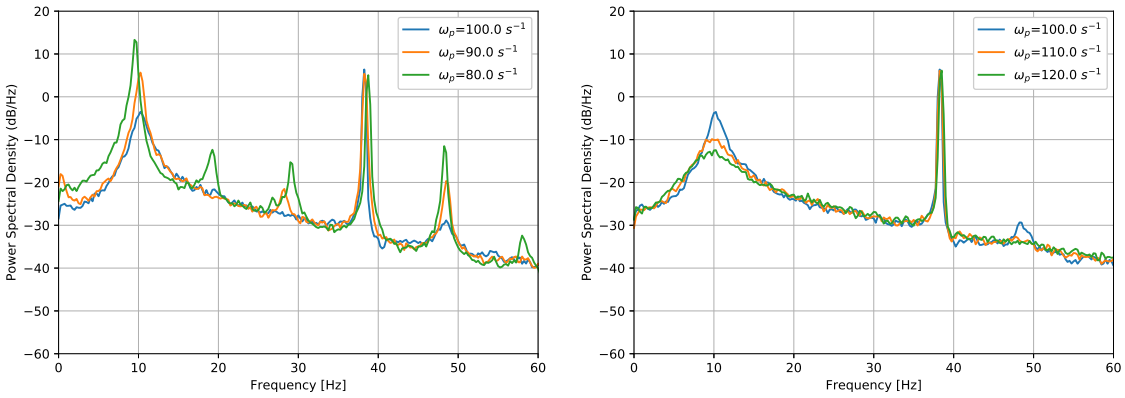

Figure 4.8. PSD comparison of the output of the model for different values of ω_p. Simulations performed for 240 seconds. On the left (right), the value of ω_p is slightly decreased (increased) with respect to the reference value $\omega_p = 100$ Hz.

In Figure 4.9, it can be observed that slightly decreasing the time constant of the slow inhibitory interneurons ω_s reduces the frequency of the low-frequency peak (orange trace). Nevertheless, decreasing ω_s even more, saturates the system, generating several frequency peaks, such as in the previous case of ω_p. Conversely, increasing the value of the ω_s only reduces the power of the low-frequency peak. Larger values of ω_s would wash out the slow-frequency peak, as seen in the previous case of ω_p.

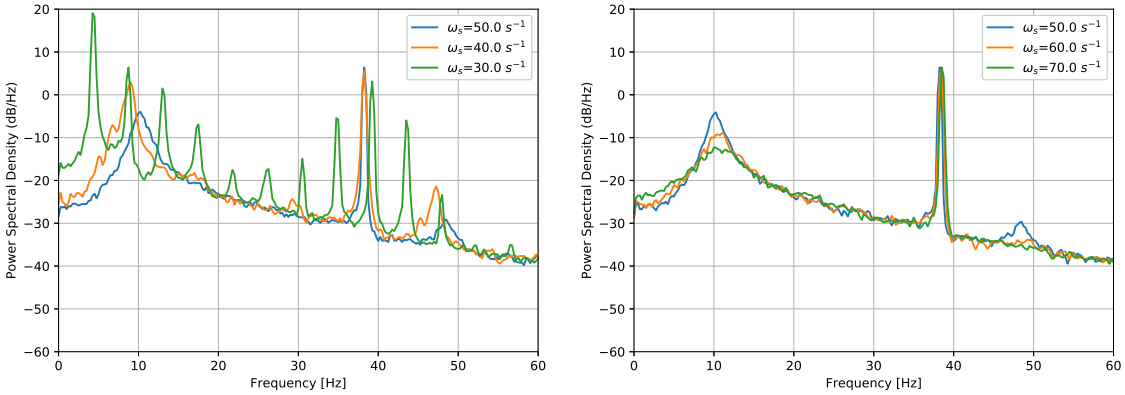

Figure 4.9. PSD comparison of the output of the model for different values of ω_s. Simulations performed for 240 seconds. On the left (right), the value of ω_s is slightly decreased (increased) with respect to the reference value $\omega_s = 50$ Hz.

The test of τ_f (Figure 4.10) shows that the slow-frequency peak, the position of the high-frequency peak moves to lower frequencies when increasing tau_f, as one can observe in Figure 4.10. Larger values

of τ_f increase the fatigue levels of the population, so fast activity cannot emerge, being equivalent to the time course of GABAergic inhibitory feedback [2].

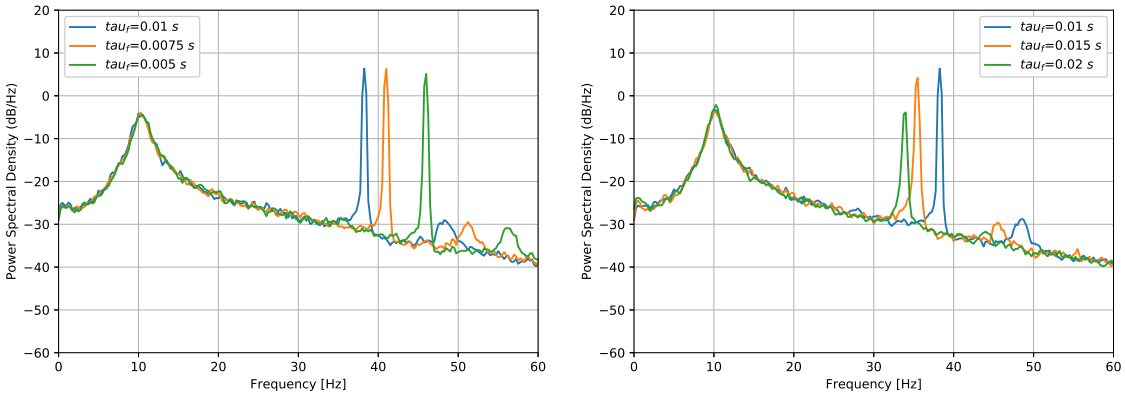

Figure 4.10. PSD comparison of the output of the model for different values of τ_f. Simulations performed for 240 seconds. On the left (right), the value of τ_f is slightly decreased (increased) with respect to the reference value $\tau_f = 10$.

When ω_f is changed, the slow-frequency peak remains fixed. Regarding the high-frequency peak, the value of ω_f affects the position of the high-frequency peak, as one can observe in Figure 4.11. If one keeps increasing ω_f the same situation as in the case of τ_f is observed.

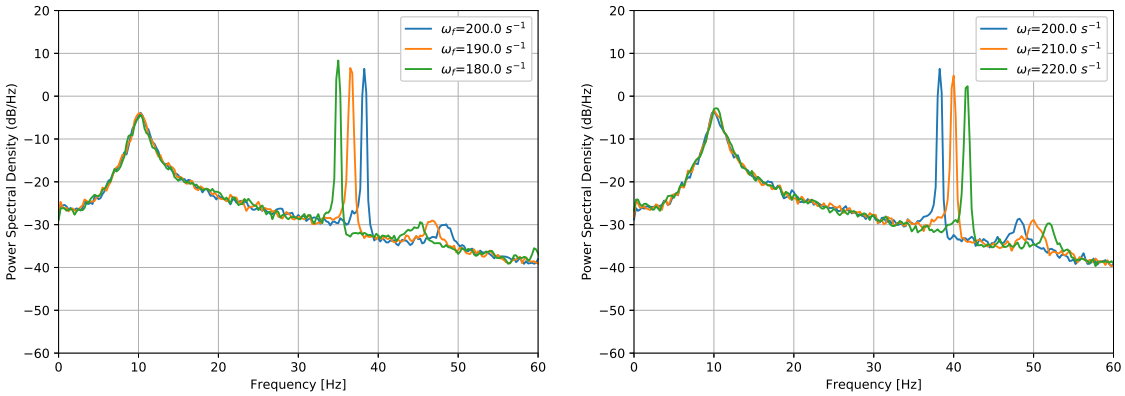

Figure 4.11. PSD comparison of the output of the model for different values of ω_f. Simulations performed for 240 seconds. On the left (right), the value of ω_f is decreased (increased) with respect to the reference value $\omega_f = 200$ Hz.

Up to now, we have found that the only parameter which slightly shifts the slow-frequency peak is ω_s. While, as predicted in the literature, the parameters that better tune the fast frequency are τ_f and ω_f.

At this stage, I proceed to present the results of the PAC and CFD analysis.

4.1.2. Analysis of the PAC and CFD

In this subsection the results of the calculated the cross-frequency correlation (CFC) and cross-frequency directionality (CFD) are presented.[1].

The same parameters, as in the previous section, have been tested (except ω_p, changing the parameter did not present any interesting feature) It is worth mentioning that it only the value of the parameters which assure the multiple peaks result in the power spectrum have been varied.

According to the main study which is being followed, the strength of PAC should change through tuning the coupling parameters C_{fs} and C_{fp}. In addition, PAC will disappear if the time constant τ_f is increased, since fast activity is suppressed [2]. Our results prove these behaviors.

Both cross-frequency coupling (CFC) and cross-frequency directionality analysis have been performed using the same signal as alpha-reference and as gamma amplitude signal. The frequency sampling rate is 1000 Hz. Regarding the frequency setup, the slow frequency ranges from 5 to 25 Hz, with a frequency step of 0.5 Hz and a bandwidth of 2 Hz . On the other hand, the fast frequency ranges from 20 to 70 Hz, with a frequency step of 2 Hz and bandwidth of 20 Hz.

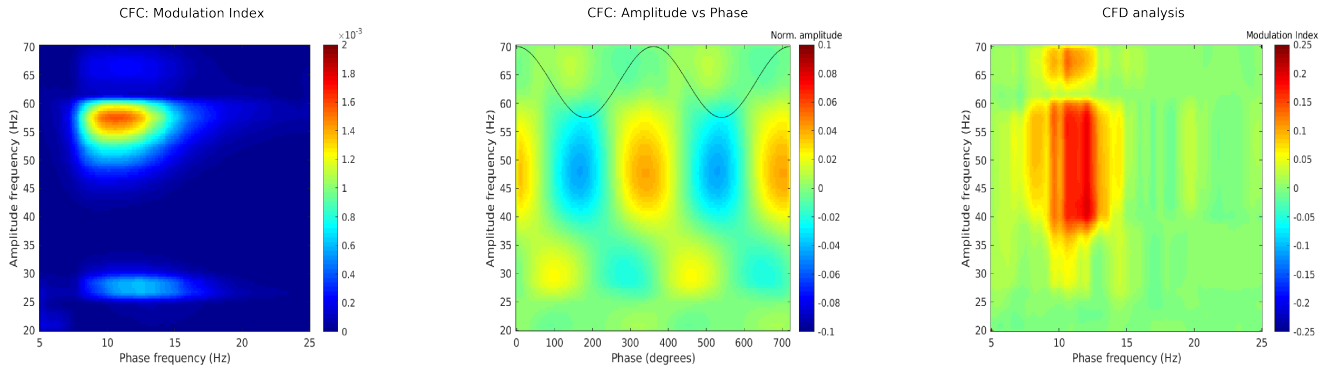

Figure 4.12. *Plots of the comodulograms. (1) Modulation index of the CFC. A higher value implies that the two frequencies are coupled between the amplitude of the fast frequency and the phase of the slow oscillation. (2) Amplitude vs. Phase of the CFC. On the x-axis is represented the phase of the slow oscillation. The black trace represents the low-pass filtered signal. On the y-axis, the amplitude of the fast frequency is again represented. A higher value of the normalized amplitude indicates that the power of the fast-oscillation at the given frequency is large. (3) Modulation index of the CFD. A positive modulation index implies that the amplitude of the fast frequency is modulated by the phase of the slow activity. A negative MI indicates the opposite.*

In Figure 4.12, it can be observe that the three comodulograms resulting from using the default parameters of the model. The first and the second represent the cross-frequency coupling (CFC), while the last one accounts for the cross-frequency directionality (CFD). We have employed the same normalized amplitude color map for each representation.

On the left of Figure 4.12 it can be seen that there is a phase-amplitude coupling (PAC) between the slow ($\sim$ 10 Hz) and fast oscillation ($\sim$ 57 Hz), respectively. It is interest to remark that the fast frequency of the peak from the PSDs representations ($\sim$ 37 Hz) is not the same as the fast frequency of the PAC ($\sim$ 57 Hz)

The amplitude vs. phase CFC indicates in which slow-frequency phase is located the larger amplitude of the gamma oscillations, being the band of 43 to 56 Hz the more powerful. Here it is also interesting to notice that there is almost in-phase synchronization between the amplitude of the fast activity and the phase of the slow oscillation (the slow oscillation positive (negative) peak coincides with the maximum (minimum) of the fast activity amplitude power.

[1]The MATLAB codes employed to calculate and represent the results of the CFC and the CFD have been provided by Victor López-Madrona

With respect to the cross-frequency directionality, it is important to observe that the modulation index is always positive, indicating that the slow oscillation modulates the fast activity (4.12, right). In fact, this behavior is maintained when tuning the selected parameters. So, we can confirm that none of the analyzed parameters can be tuned to achieve a modulation of the fast over the slow oscillation. In addition, it is interesting to notice that the bands of frequency with highest modulation index are approximately 10 to 12.5 Hz and 40 to 60 Hz, for the slow and fast oscillation respectively.

Having explained the CFC and CFD plots for the default parameters, we proceed to analyze the results of tuning the parameters.

With respect to C_{fp}, Figure 4.13 shows that there is not phase-amplitude coupling if C_{fp} is reduced to 0. Conversely, increasing the parameter does not remove the coupling, but the intensity is slightly weakened. With relation to Figure 4.14, it is worth mentioning that increasing C_{fp} implies an increase on the power of the amplitude of the fast oscillation, which also completely synchronizes to be in-phase with the slow oscillation. In other words, the envelope of the amplitude of the fast oscillations matches the phase of the slow ones. Regarding the CFD analysis, if there is no synaptic gain from the fast inhibitory to the pyramidal neurons, there is no synchronization between oscillations (Figure 4.15). Additionally, an increase of the synaptic gain leads to a broader slow-frequency band with a large CFD modulation index.

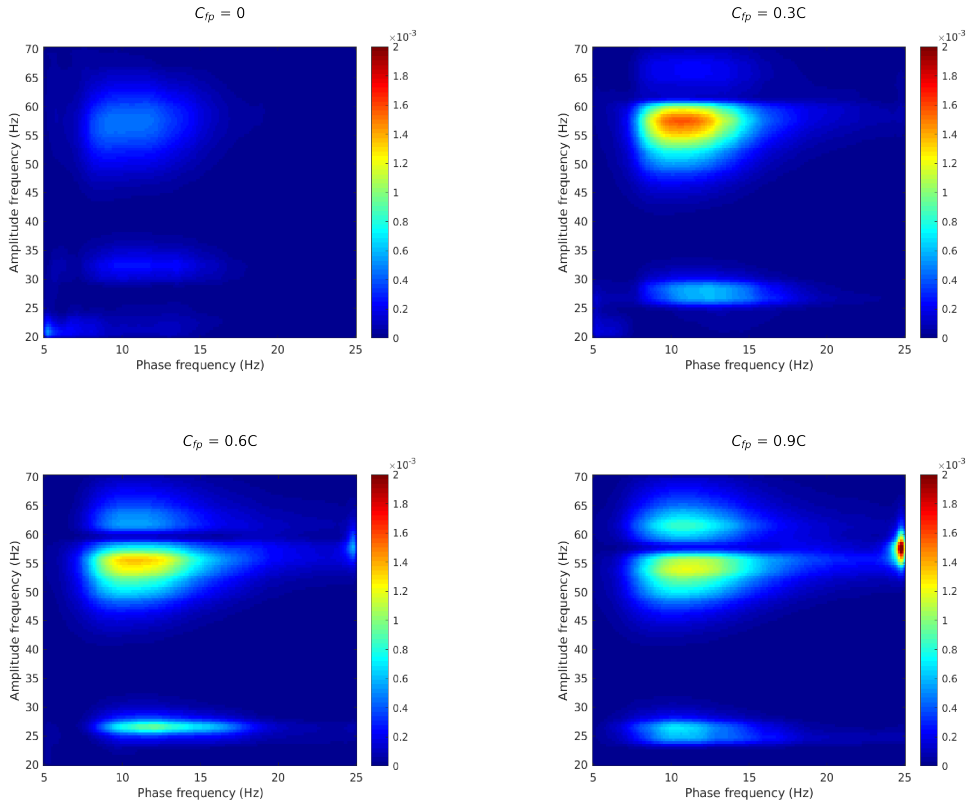

Figure 4.13. Influence of the parameter C_{fp} on the modulation index of the phase-amplitude correlation (PAC) of the output of the model.

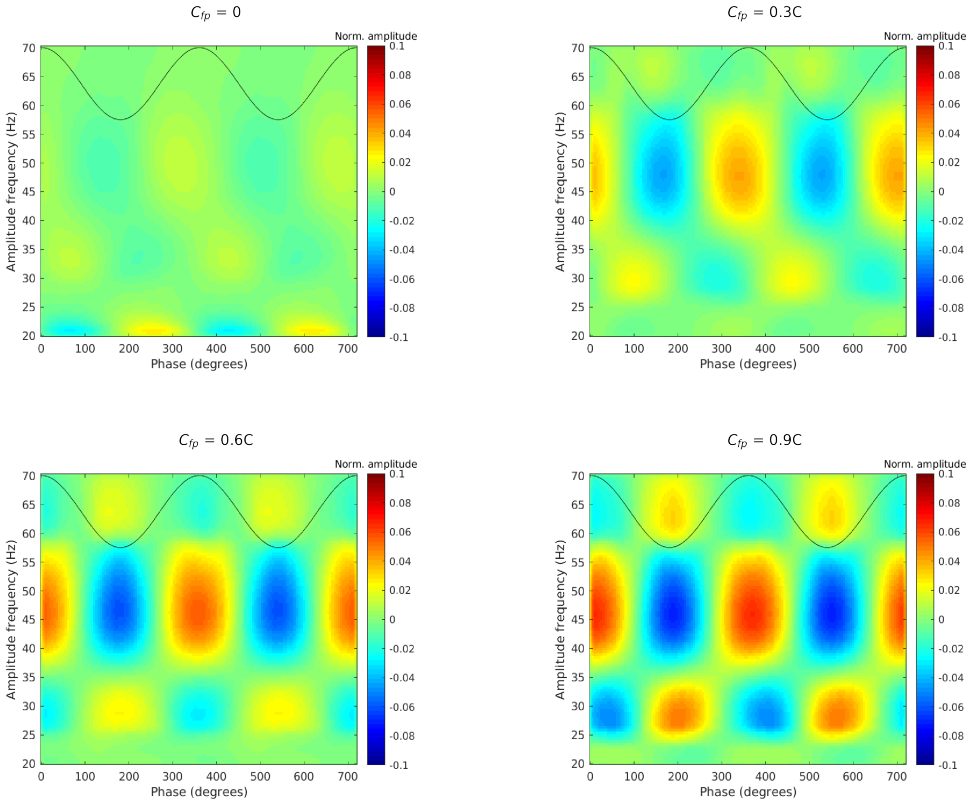

Figure 4.14. Influence of the parameter C_{fp} on the amplitude vs. phase CFC of the output of the model.

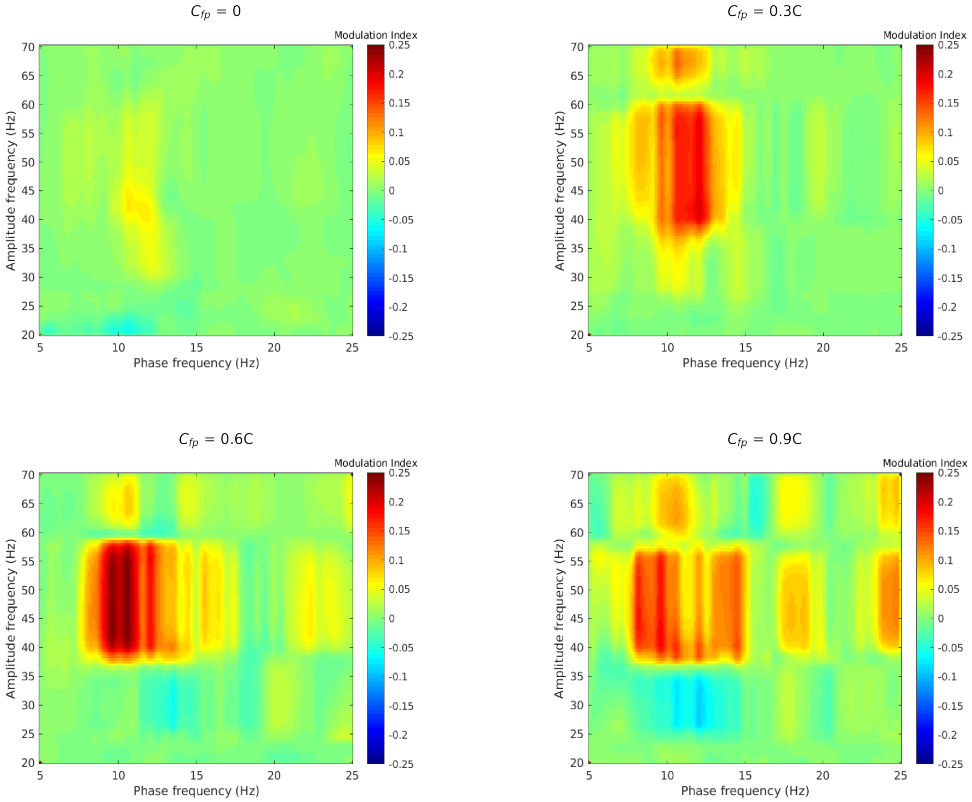

Figure 4.15. Influence of the parameter C_{fp} on the modulation index of the cross-frequency directionality (CFD) of the model.

It can be seen in Figure 4.16 that as C_{fs} is increased, the PAC intensity level rises, as stated in [2]. Nevertheless, we have also found two behaviors which are not mentioned in that article. First, Figure 4.17 shows that the changes in C_{fs} can vary the synchronization between the amplitude of the fast oscillation and the phase of the slow activity, as in the case of C_{fp}. Decreasing C_{fs} facilitates the in-phase state, while increasing it, promotes an anti-phase synchronization. Moreover, in Figure 4.18 it can be seen that the slow frequency with the higher CFD modulation index suffers a slightly displacement towards faster frequencies.

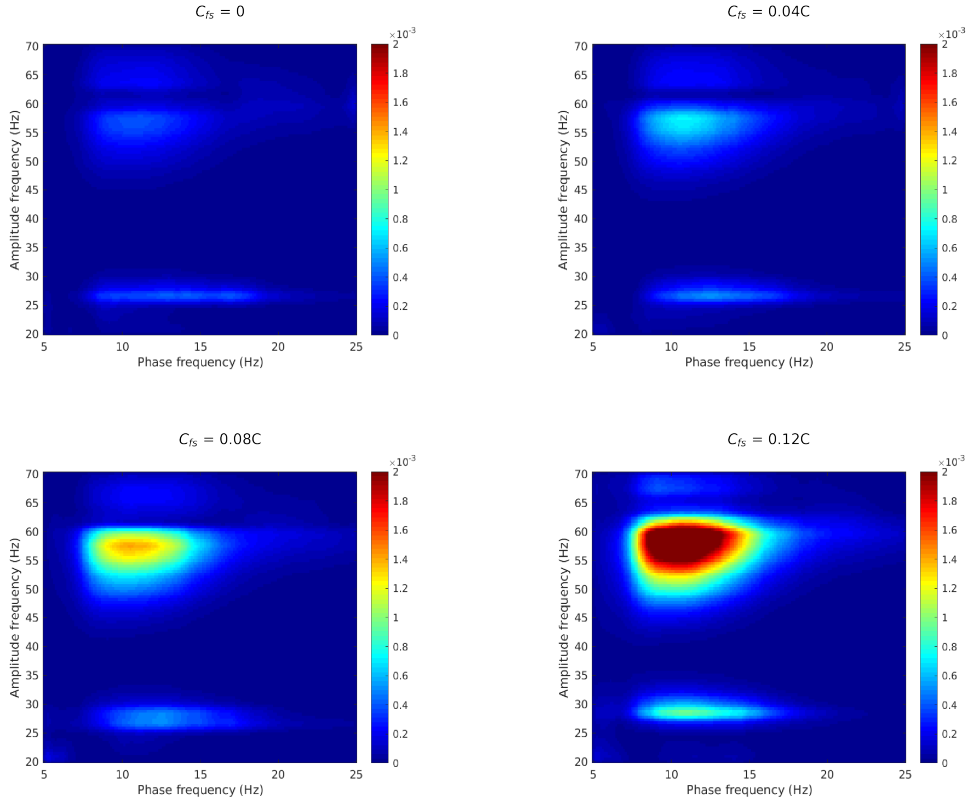

Figure 4.16. Influence of the parameter C_{fs} on the modulation index of the phase-amplitude correlation (PAC) of the output of the model. This particular representation is also shown in [2].

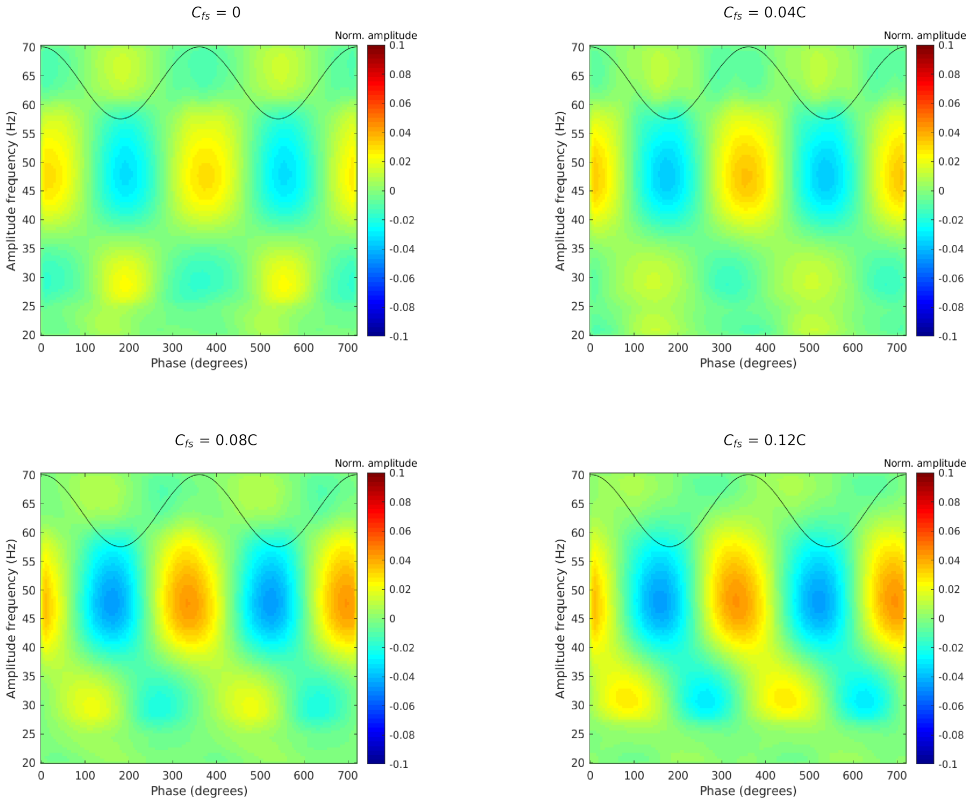

Figure 4.17. Influence the parameter C_{fs} on the amplitude vs. phase CFC on the output of the model.

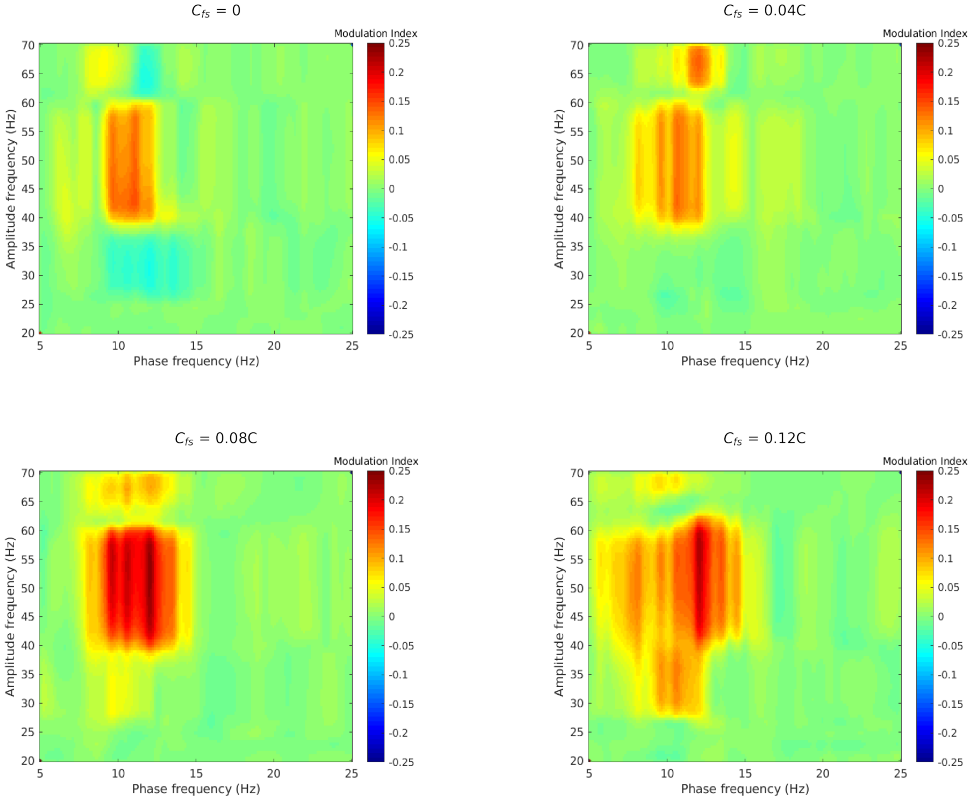

Figure 4.18. Influence of the parameter C_{fs} on the modulation index of the cross-frequency directionality (CFD) of the model.

Concerning C_{pf}, neither the CFC, nor the CFD analysis suffer any significant modification when tuning the parameter, thus results are not shown.

A change in τ_f entails an interesting behavior. In Figure 4.19 it can be seen that the value of the fast frequency coupled to the the phase of the slow activity is higher when τ_f is increased. To understand this behavior one should look again into Figure 4.10, where it is appreciable that apart form the more powerful frequency peaks, there is another less powerful peak, called modulatory component, ranging from ~ 45 to ~ 55 Hz depending on the value of τ_f. The modulatory component indicates that the amplitude of the fast-frequency peak is modulated by the slow-frequency peak at 10 Hz (observe in Figure 4.10 that the difference between the position of the fast-frequency peak and the modulatory component is 10 Hz for all the cases). This modulation frequency is related to the frequency coupled with the slow activity. Particularly, when $\tau_f = 5$ ms there is another frequency (roughly at 35 Hz) with a high CFC modulation index. This maximal value is also related with the other modulatory component, which is less visible in Figure 4.10 because it is suppressed by the activity of the other populations and noise. As previously explained, increasing τ_f results in a suppression of the fast activity which leads to the disappearance of the phase-amplitude coupling. This can be observed in Figure 4.20 and Figure 4.21.

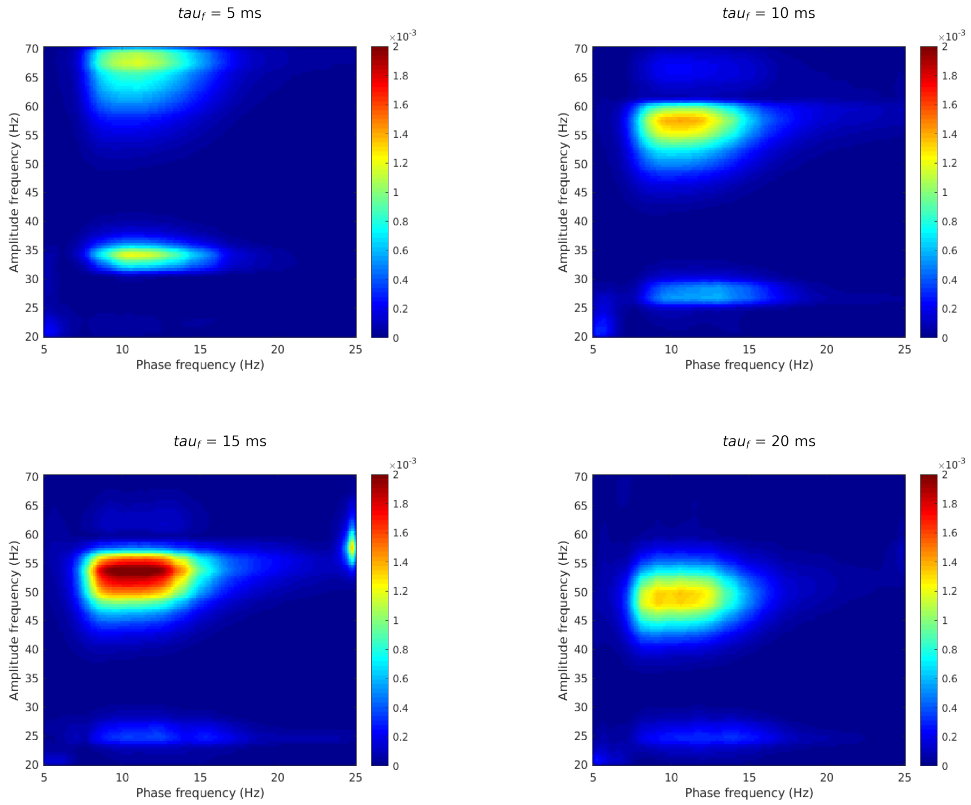

Figure 4.19. Influence of the parameter τ_f on the modulation index of the phase-amplitude correlation (PAC) of the output of the model.

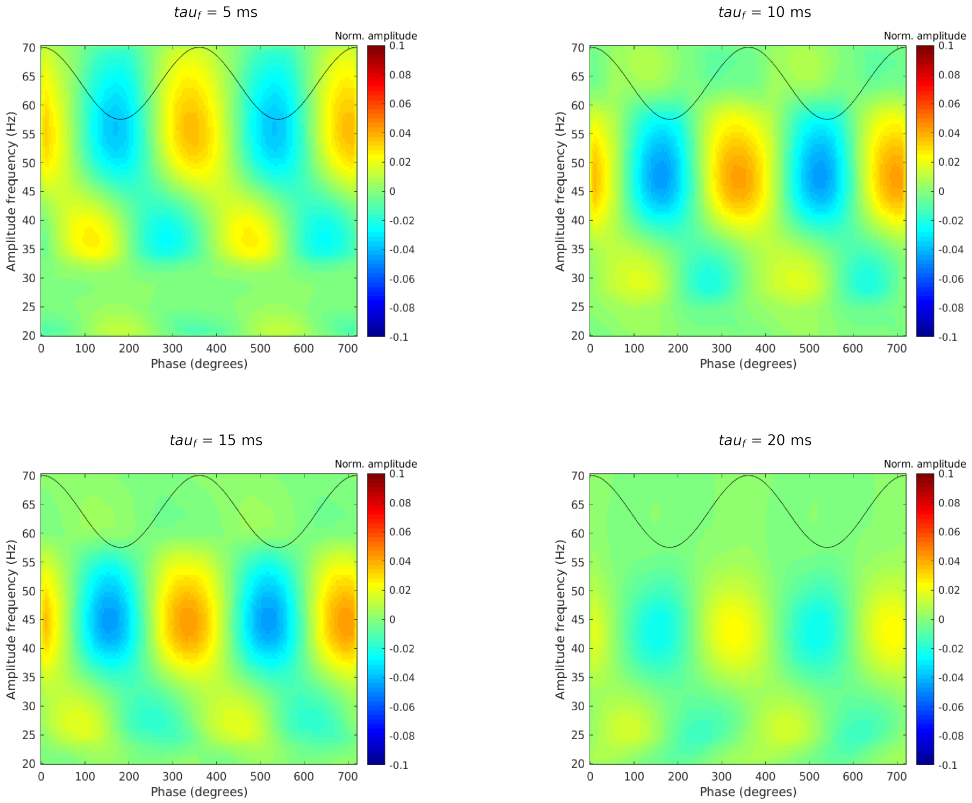

Figure 4.20. Influence of the parameter τ_f on the amplitude vs. phase CFC on the output of the model.

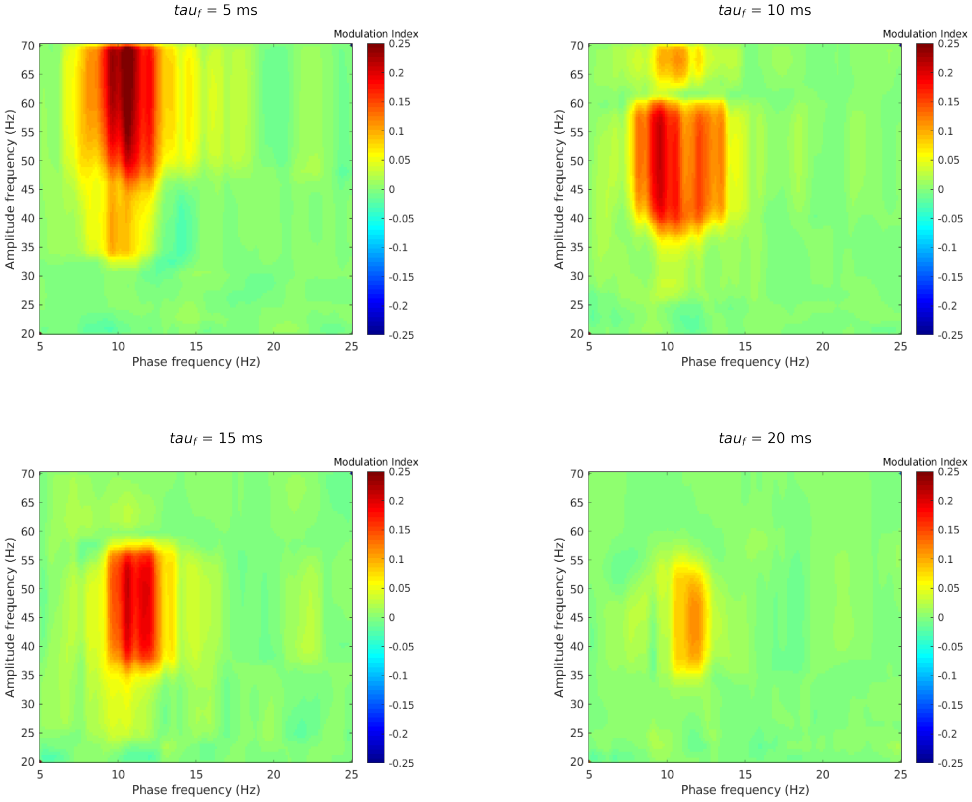

Figure 4.21. Influence of the parameter τ_f on the modulation index of the cross-frequency directionality (CFD) of the model.

Regarding the variation of ω_s and ω_f, no interesting facts have been found related to the cross-frequency directionality. In Figure 4.22, it can seen that slightly decreasing ω_s can lead to a stronger phase-amplitude coupling. Concerning ω_f, as can be seen in Figure 4.23, PAC is stronger for higher values.

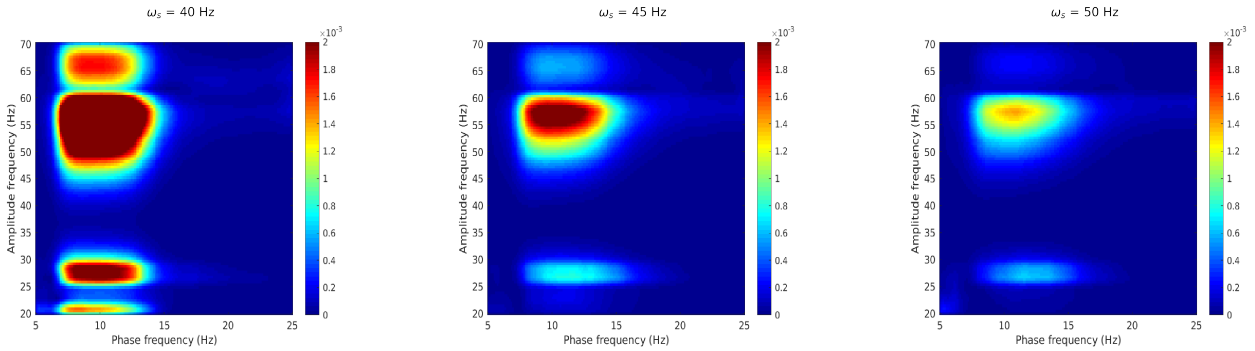

Figure 4.22. Influence of tuning the parameter ω_s on the modulation index of the phase-amplitude correlation (PAC) of the output of the model.

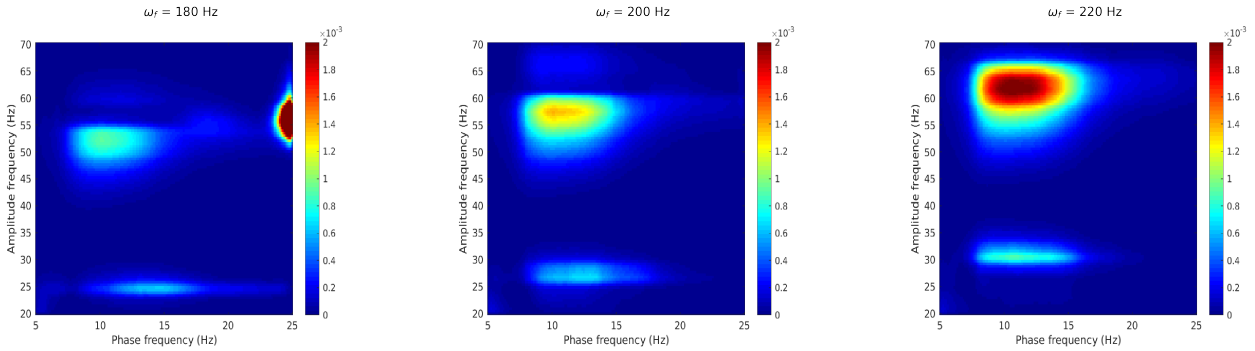

Figure 4.23. Influence of the parameter ω_f on the modulation index of the phase-amplitude correlation (PAC) of the output of the model.

As predicted by the previous study [2], we have obtained that changing C_{fs} is sufficient to modulate the intensity of PAC, with very little modifications on the frequency peaks of the output (see Figure 4.6).

We have also seen that by changes in C_{fs} and C_{fp} we can change the synchronization between the amplitude of the fast oscillation and the phase of the slow activity (Figure 4.14 and Figure 4.17).

Furthermore, it is important to remark that tuning a parameter in order to change a frequency peak can lead to an undesired variation of the PAC and vice versa. An example of such problem is the case of increasing τ_f, or decreasing ω_f, in order to reduce the value of the fast frequency peak. Since this shift also leads to a lost of the PAC of the system.

4.2. A NMM with N nodes

The model developed for a specific number of nodes has been simulated in Python 3, using a fourth order Runge-Kutta method, with a time step of 0.0001 seconds. Each simulation is performed for 61 seconds unless otherwise specified, removing the first second to avoid transient dynamics. The signals are normalized to zero mean. It is worth mentioning that the model considers that the connection between nodes occurs via pyramidal neurons.

Case of 2 nodes

Although the model provides five out of the theoretically proposed six different coupling, we have only focus on the PAC. In such a case, the mean input noise level of the nodes are $P_1 = 0$, to deactivate the fast oscillation in the first node; and $P_2 = 7$, in order to trigger a steady-state gamma band oscillation [3]. The rest of the values of the parameters used in the model can be found in Table 4.2 (Appendix B).

Once again, the first step consists in testing the developed model to ensure its performance. Figure 4.24 shows the temporal traces of the membrane potential of the pyramidal population of each node. Phase-phase coupling (PPC) can be observed, but the PAC is not appreciable. In order to solve this problem, the output of each node has been decomposed into a fast oscillation (FO) and a slow oscillation (SO), by using a high-pass, filtering frequencies below the cut-off frequency $f_c = 15$ Hz; or a low-pass, filtering frequencies above f_c. A second-order Butterworth filter has been employed (Figure 4.25). After filtering, local PAC is observed in node 2. It can be visually assessed that the frequency is constant and the envelope of the amplitude of the FO is in phase with the SO. As a result, there is a cross node PAC between both nodes.

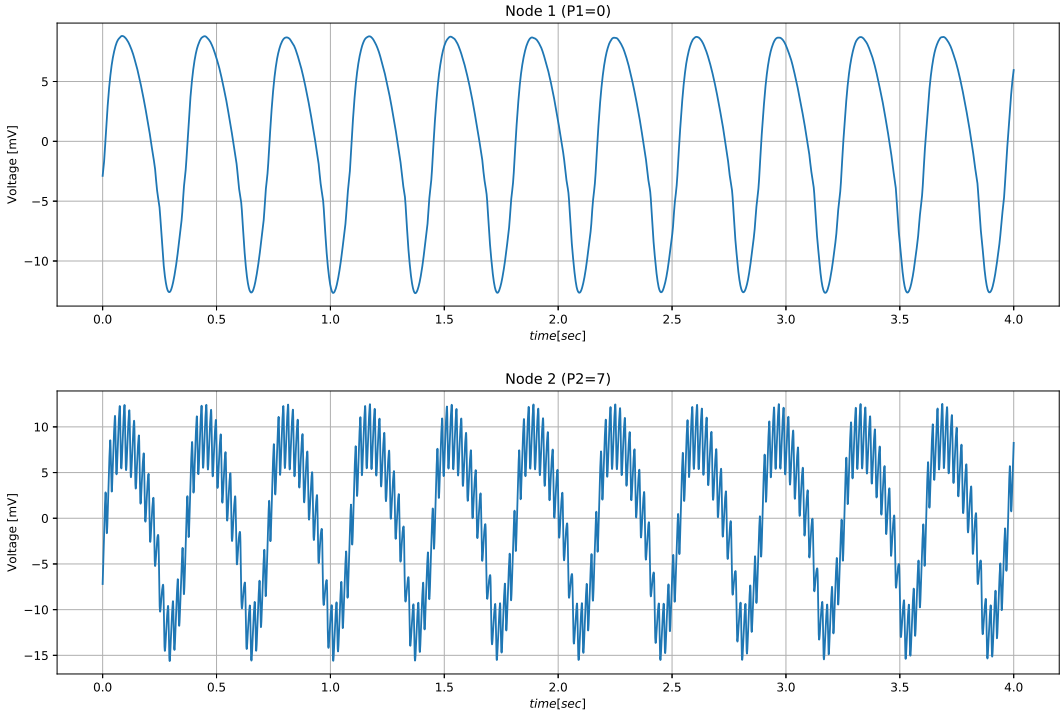

Figure 4.24. Temporal traces of the output of each node. Simulations performed for 5 seconds removing the first second.

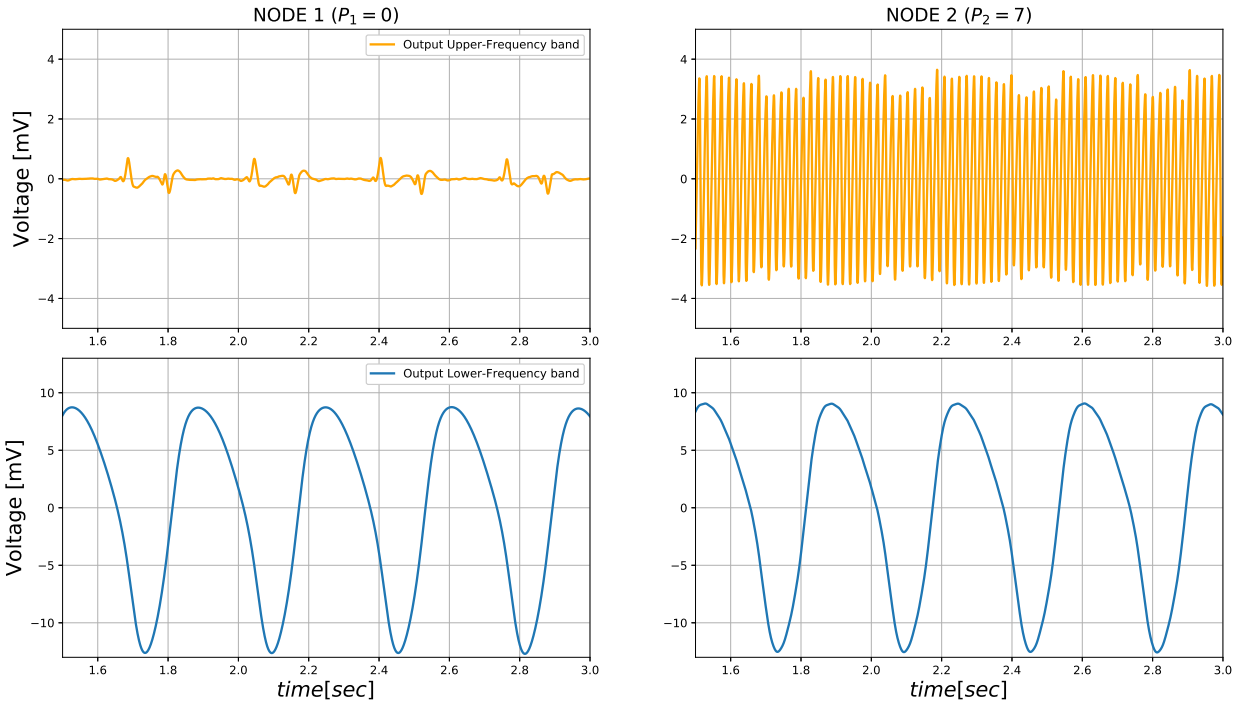

Figure 4.25. Top: Fast Oscillations (FO). Bottom: Slow Oscillations (SO). Representation of the PAC simulation. Local PAC between the FO and SO of node 1, and cross-node PAC between FO of node 2 and SO of node 1 are observable. Represented from [3].

Then, it is evaluated the response of the model to varying the synaptic gains between the two nodes (K_{12}, K_{21}). In order to do so, CFD and PAC have been analyzed. Only four cases have been assessed: the default case, $(K_{12}, K_{21} = (40, 40)$; the two cases in which one node is not connected to the other one, $(K_{12}, K_{21} = (0, 40)$ and $(K_{12}, K_{21} = (40, 0)$; and the case in which both connections are increased, $(K_{12}, K_{21} = (120, 120)$.

Figure 4.26 shows the PSDs of the outputs from nodes 1 and 2 when tuning K_{12} and K_{21}. Peaks appear in ~ 3 Hz and ~ 47 Hz bands, which indicate stationary oscillatory activity. If the influence from node 2 to node 1 is removed ($K_{21} = 0$), there would not be any activity in node 1, since at least one source of input noise is required. For the other three cases, CFC and CFD have been assessed between the following signals:

- The membrane potentials of the pyramidal population (output) of both nodes.
- The output of node 1 and the fast inhibitory interneuron postsynaptic potential of the of node 2.
- The output of node 2 and the fast inhibitory interneuron postsynaptic potential of the of node 1.

The frequency sampling rate is 10000 Hz. Regarding the frequency setup, the slow frequency ranges from 2 to 6 Hz, with a frequency step of 0.5 Hz and a bandwidth of 1 Hz . On the other hand, the fast frequency ranges from 35 to 60 Hz, with a frequency step of 1 Hz and bandwidth of 10 Hz.

In the case $(K_{12}, K_{21} = (0, 40)$, we do not observe PAC, confirming that in order to obtain cross-frequency coupling there should be a feedback between the nodes.

As expected, the cross-frequency coupling is larger in the three pairs of signals analyzed when the connections are increased. Nevertheless, in none of the cases we found a directionality of the amplitude of the fast oscillation modulating the phase of the slow activity. Thus, since there is no interesting features reported, we do not show the figures.

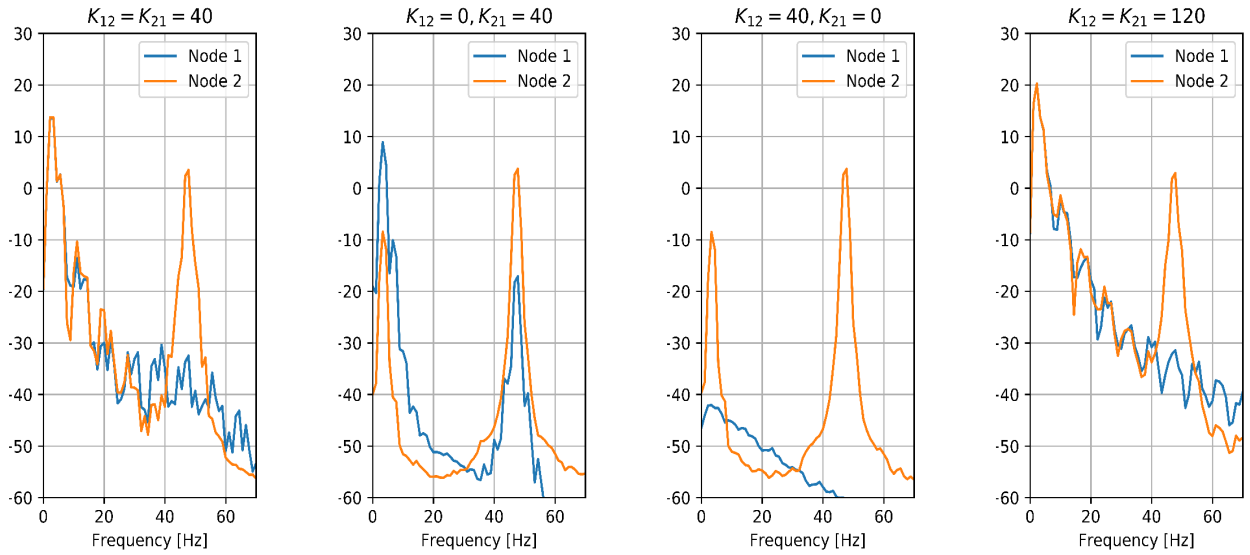

Figure 4.26. Comparison of PSDs for the 4 different cases assessed shifting the between node synaptic gain.

Case of 3 nodes

We also show the results that confirm the usability of the computed NMM for a specific number of nodes, particularly for three nodes. The three nodes of the model are featured with the same structural and connectivity parameters as indicated in Table 4.2, except the average time constant of self-synaptic decay in fast inhibitory interneurons, which are $\tau_1 = 10$ ms, $\tau_2 = 5$ ms, and $\tau_3 = 20$ ms; and the mean input noise level $P = \alpha$. We have limited ourselves to two cases of P parameters sets. First, $(P_1, P_2, P_3) = (0, 4.5, 4.5)$, and then, $(P_1, P_2, P_3) = (0, 4.5, 7)$.

Figure 4.27 and Figure 4.28 show the results, which have been qualitatively evaluated. As in the case of two nodes, all the slow amplitude phases present phase-phase coupling (PPC). It can be seen in Figure 4.27 that the frequency of the FO2 (fast oscillation of node 2) remains nearly unchanged. Whereas its amplitude envelope is in phase with the SO2, and also SO1 and SO3, so there is PAC between the FO2 and the SOs. This behavior is also observed in the case of 2 nodes. Interesting behavior occurs in node 3. It is clear that the FO3 frequency is larger when the SO3 reaches its maximum, and lower in the valleys of the SO3. Also, the amplitude is systematically larger in the positive phases of the SO3. The amplitude remains almost constant in each slow-cycle, nevertheless, it changes with an unknown pattern for each SO cycle. In essence, in node 3 we can observe a strong phase-frequency coupling (PFC) and a weak PAC. Also, there is an amplitude-frequency coupling (AFC) from FO2 to FO3.

With respect to Figure 4.28, the main difference is that by increasing the value of P_3, the PFC disappears. Instead, the model shows an amplitude-amplitude coupling (AAC) between SO2 and SO3.

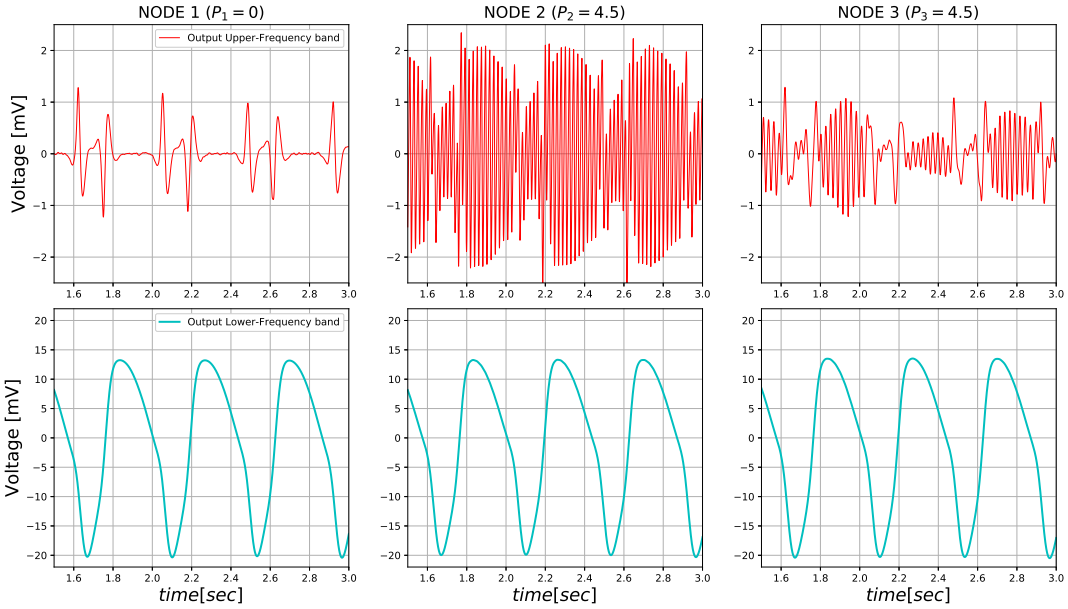

Figure 4.27. Top: Fast Oscillations (FO). Bottom: Slow Oscillations (SO). Representation of a 3 nodes simulation using the first set of P parameters.

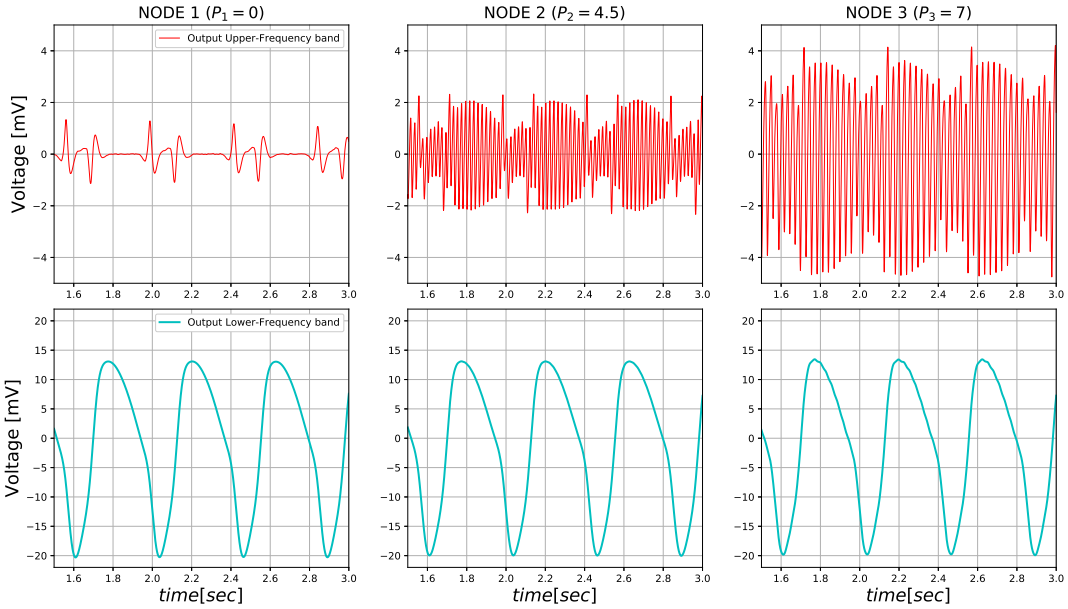

Figure 4.28. Top: Fast Oscillations (FO). Bottom: Slow Oscillations (SO). Representation of a 3 nodes simulation using the second set of P parameters.

Chapter 5

Conclusion

In this master thesis, I have reproduced the neural mass model of a single node proposed in Ref. [2], comprised of four different populations: pyramidal neurons, excitatory interneurons, slow inhibitory interneurons and fast inhibitory interneurons. Furthermore, I have developed a neural mass model for a given number of nodes, on the basis of the neural mass model for two nodes presented in Ref. [3].

The key goal of developing these models was to dissect how the hippocampus can carry out its complex behavior. I order to do so, we tried to replicate these processes in a computational model, and reproduce the experimentally obtained results. In order to analyze the models, we have varied some parameters. We also have focus on the limiting cases, to verify that the results of the model were biologically plausible.

Particularly, concerning the single node NMM, we have studied how to modulate the position of the frequency peaks produced by the model and the conditions for which the phase-amplitude coupling (PAC) occurred. Regarding the modulation of the position of the peaks, we have shown that the more suitable parameters to change are the time constant of the slow inhibitory population (ω_s) to modulate the low-frequency peak position; and the time constant of the dynamics in the self-feedback (τ_f), to modulate the high-frequency peak position. Concerning the PAC, we have mainly found that changes in C_{fs} and C_{fp} lead to changes in the synchronization of the fast frequency amplitude and the slow frequency phase.

Moreover, cross-frequency directionality (CFD) has been assessed, without finding any set of parameters to obtain a result in which the amplitude of gamma oscillations modulates the phase of theta, phenomena that Ref. [1] found to occur in the hippocampus. There are several reasons why we have not found a way to modulate this behavior. We suspect that it might be due to the configuration of the connections between the different populations, that could be different from the real one. Another reason can be the existence of a pacemaker in the CA3, the Septum [41], which mis not included in the model. Furthermore, it might be that the resonance is not represented with the the model. Resonance can enhance certain frequencies rhythms in a neuron. For instance, a stronger gamma resonance would easily activate that frequency, being able to affect the phase of theta.

Concerning the two-nodes NNM, we have analyzed the influence of the gain between nodes, and test that the model works for more than two nodes.

Future prospects

This project could have been widely extended, since there are many potential aspects to improve the study. First of all, more parameter sets can be analyzed. Also, the combination of changes in more than one parameter can probably lead to behaviors which have not being observed yet. Moreover, it is worthy mention the possibilities offered by the NMM of a specif number of nodes, which require a deeper study of all the possible parameters in order to modulate any given inter-node connectivity.

Furthermore, it could be interesting to explore other models, such as the proposed in Ref. [42], which presents a multiscale model of hippocampal CA3 to study theta-gamma modulation. Likewise, another computational model that achieved to reproduce the theta-gamma CFC is the presented in Ref. [43]. It takes into account the current produced by the hyperpolarization-activated cyclic nucleotide–gated (HCN) channel, which is a voltage-gated ion channel involved in sub-threshold resonance and regulating neuronal excitability. The study of these and other models could give rise to new ideas which can be added to the current model to improve its performance.

Appendix A

CFC and CFD Algorithms

The explanation of both algorithms is based on Ref. [1].

CFC Algorithm

To evaluate the CFC between the phase and the amplitude, modulation index (MI) is employed, which is based on entropy measurements. Given two signals, $x_\theta(t)$ and $x_\gamma(t)$, filtered at a slow and a fast frequency, it can be extracted the phase $x_{\theta\varphi}(t)$ and the amplitude $x_{\gamma A}(t)$, respectively, using the Hilbert transform. Next, each whole cycle in $x_{\theta P}(t)$ is divided in N bins of the same size. We define $\left\langle x_{\gamma A}(t)\right\rangle_\varphi(j)$ as the mean amplitude value at the phase bin j. Therefore, the entropy measure H, can be calculated as:

$$H = -\sum_{j=1}^{N} p_j \log p_j \qquad\qquad p_j = \frac{\left\langle x_{\gamma A}(t)\right\rangle_\varphi(j)}{\sum_{j=1}^{N}\left\langle x_{\gamma A}(t)\right\rangle_\varphi(j)} \tag{A.1}$$

The value of the MI is obtained normalizing H by the maximum entropy H_{max}, which is the case of the uniform distribution $p_j = 1/N$:

$$MI = \frac{H_{max} - H}{H} \tag{A.2}$$

Low MIs values imply a low phase-amplitude modulation, while larger MI values show a high phase-amplitude modulation. The statistical significance is assessed by a surrogate analysis, in which each surrogate is built by random shifts between the phase and the amplitude of both signals. The series are approximated to a gaussian distribution, which mean value is considered as a significance threshold.

The values of the slow and fast frequencies have being shifted to cover all values represented in each comodulogram of MIs. The bandwidth and the step of each of the axis is specific for each case. It is important to remark that the y-axis bandwidth must be fixed at least two times the frequency where the maximum theta value is expected.

CFD Algorithm

The theta phase can modulate the amplitude at gamma frequencies while or vice versa. To identify who is the driver, the directionality of the coupling can be assessed using the cross-frequency directionality (CFD) index. It is based on the phase-slope index (PSI), a measurement of causality between time series. The aim is that, if the oscillation of a signal is modulating another with a time delay, the phase difference between them changes consistently with the frequency. The slope of the phase is obtained as a function of the frequency, and the sign indicates who is the driver. The employed signals are $X(t)$: Fourier transform of the original signal, and $X^{\nu}_{\gamma A}$: Fourier transform of the power envelope of the other signal at gamma frequency. The other interesting parameters are: $C(\nu, f_j)$: complex coherence, f_j: theta frequency under study, S: number of divisions of the signal, β: bandwidth for which the phase slope is measured, and Δf: the resolution. Thus, the CFD is defined as:

$$\psi(\nu, f_j) = Im\left(\sum_{f_j+\beta/2}^{f_j+\beta/2} C^*(\nu, f_j)C(\nu, f_j + \Delta f)\right) \qquad C(\nu, f_j) = \frac{\sum_{s=1}^{S} X^S (X^{\nu,s}_{\gamma A})^*}{\sqrt{\sum_{s=1}^{S} |X^S|^2 \sum \left|X^{\nu,s}_{\gamma A}\right|^2}} \quad \text{(A.3)}$$

The same steps than in the MI of the CFC have been followed to provide statistical significance. The result of the CFD can be positive or negative, meaning that the phase of the slow rhythm modulates the fast oscillation (FO) and vice versa, respectively. Nevertheless, in order to assess whether our results are significant or not, the value of the CFC MI is required to be high.

Appendix B

Tables of parameters

Table B.1. Model parameters. Variables for a given node α.

Notation	Parameter Interpretation
$C_{\alpha u u'}$	Synaptic gain from population u to u' population
$C_{\alpha f f}$	Synaptic gain of fast inhibitory interneurons self-feedback
${\omega_{\alpha u}}^{-1}$	Average time constant of u population membrane potential [sec]
${\omega_{\alpha \beta u}}^{-1}$	Average time constant of between nodes α and β membrane potential of u population [sec]
${\omega_{\alpha n}}^{-1}$	Average time constant of the filtered noise [sec]
$G_{\alpha u}$	Average dendritic gains of u population [mV]
$G_{\alpha \beta u}$	Average dendritic gains of between node u population [mV]
$G_{\alpha n}$	Average dendritic gains of the filtered noise [mV]
$K_{\alpha u}$	Noise excitation weight for u population
$K_{\alpha \beta}$	Synaptic gain from node β to node α
$\tau_{\alpha f}$	Average time constant of self-synaptic decay in fast inhibitory interneurons [sec]
P_α	Mean input noise level $[Hz]$
σ_α^2	Variance of white noise $[Hz^2]$

Table B.2. Model parameters. Fixed values.

Parameter interpretation	Notation	Value
Expected spiking threshold voltage [mV]	V_θ	5
Half-maximum firing rate [Hz]	ν_{max}	2.5
Variance of membrane potential over individual neurons in the population $[mV^{-1}]$	r	1.12

Table B.3. Model parameters of a one node NMM. Fixed values. Values taken from [2]

Parameter interpretation	Notation	Value
Expected spiking threshold voltage [mV]	V_θ	6
Half-maximum firing rate [Hz]	ν_{max}	2.5
Variance of membrane potential over individual neurons in the population $[mV^{-1}]$	r	0.56
Synaptic gain from excitatory interneurons unit to pyramidal unit	C_{qp}	$C = 135$
Synaptic gain from pyramidal unit unit to excitatory interneurons unit	C_{pq}	$0.8C = 108$
Synaptic gain from slow inhibitory interneurons unit to pyramidal unit	C_{sp}	$0.25C = 33.75$
Synaptic gain from pyramidal unit to slow inhibitory interneurons unit	C_{ps}	$0.25C = 33.75$
Synaptic gain from slow inhibitory interneurons unit to pyramidal unit	C_{fp}	$0.3C = 40.5$
Synaptic gain from pyramidal unit to fast inhibitory interneurons unit	C_{pf}	$0.1C = 13.5$
Synaptic gain from fast inhibitory interneurons unit to slow inhibitory interneurons unit	C_{fs}	$0.08C = 10.8$
Synaptic gain of fast inhibitory interneurons self-feedback	C_{ff}	$0.72C = 97.2$
Average time constant of pyramidal population membrane potential [sec]	$T_p = \omega_p^{-1}$	100^{-1}
Average time constant of excitatory interneurons population membrane potential [sec]	$T_q = \omega_q^{-1}$	100^{-1}
Average time constant of fast inhibitory interneurons population membrane potential [sec]	$T_f = \omega_f^{-1}$	200^{-1}
Average time constant of slow inhibitory interneurons population membrane potential [sec]	$T_s = \omega_s^{-1}$	50^{-1}
Average dendritic gains of between pyramidal population [mV]	G_p	3.2
Average dendritic gains of between excitatory interneuron population [mV]	G_q	3.2
Average dendritic gains of between fast inhibitory population [mV]	G_f	50
Average dendritic gains of between slow inhibitory population [mV]	G_s	22
Average time constant of self-synaptic decay in fast inhibitory interneurons unit [sec]	τ_f	0.01
Modulatory input of fast inhibitory interneurons unit [Hz]	P_f	1
Mean of white noise [Hz]	ν_p	2.5
Variance of white noise $[Hz^2]$	σ_p^2	1.65
Noise gain	K_p	$C = 135$

Table B.4. Model parameters of the NMM for a specific number of nodes. Fixed values. Values taken from [3]. The average time constant of the self-synaptic decay $\tau_{\alpha f}$ and the mean input noise level P_α are specified for each case.

Parameter interpretation	Notation	Value
Expected spiking threshold voltage [mV]	V_θ	5
Half-maximum firing rate [Hz]	ν_{max}	2.5
Variance of membrane potential over individual neurons in the population $[mV^{-1}]$	r	1.12
Synaptic gain from excitatory interneurons unit to pyramidal unit	$C_{\alpha qp}$	$C = 135$
Synaptic gain from pyramidal unit unit to excitatory interneurons unit	$C_{\alpha pq}$	$0.8C = 108$
Synaptic gain from slow inhibitory interneurons unit to pyramidal unit	$C_{\alpha sp}$	$0.25C = 33.75$
Synaptic gain from pyramidal unit to slow inhibitory interneurons unit	$C_{\alpha ps}$	$0.25C = 33.75$
Synaptic gain from slow inhibitory interneurons unit to pyramidal unit	$C_{\alpha fp}$	$0.3C = 40.5$
Synaptic gain from pyramidal unit to fast inhibitory interneurons unit	$C_{\alpha pf}$	$0.2C = 27$
Synaptic gain from fast inhibitory interneurons unit to slow inhibitory interneurons unit	$C_{\alpha fs}$	$0.08C = 10.8$
Synaptic gain of fast inhibitory interneurons self-feedback	$C_{\alpha ff}$	$C = 135$
Average time constant of pyramidal population membrane potential [sec]	$T_p = \omega_{\alpha p}^{-1}$	10^{-1}
Average time constant of excitatory interneurons population membrane potential [sec]	$T_q = \omega_{\alpha q}^{-1}$	100^{-1}
Average time constant of fast inhibitory interneurons population membrane potential [sec]	$T_f = \omega_{\alpha f}^{-1}$	200^{-1}
Average time constant of slow inhibitory interneurons population membrane potential [sec]	$T_s = \omega_{\alpha s}^{-1}$	50^{-1}
Average dendritic gains of between pyramidal population [mV]	$G_{\alpha p}$	0.32
Average dendritic gains of between excitatory interneuron population [mV]	$G_{\alpha q}$	3.2
Average dendritic gains of between fast inhibitory population [mV]	$G_{\alpha f}$	50
Average dendritic gains of between slow inhibitory population [mV]	$G_{\alpha s}$	22
Variance of white noise $[Hz^2]$	σ_α^2	0.5
Noise excitation weight for pyramidal neurons	$K_{\alpha p}$	40
Noise excitation weight for fast inhibitory neurons	$K_{\alpha f}$	108
Average time constant of between nodes α and β membrane potential of u population [sec]	${\omega_{\alpha\beta u}}^{-1}$	10^{-1}
Average time constant of the filtered noise [sec]	${\omega_{\alpha n}}^{-1}$	10^{-1}
Average dendritic gains of between node u population [mV]	$G_{\alpha\beta u}$	0.32
Average dendritic gains of the filtered noise [mV]	$G_{\alpha n}$	0.32
Synaptic gain from node β to node α	$K_{\alpha\beta}$	40

Bibliography

[1] Victor Lopez-Madrona, Efren Álvarez Salvado, David Moratal, Oscar Herreras, Ernesto Pereda, Claudio R Mirasso, and Santiago Canals. Gamma oscillations coordinate different theta rhythms in the hippocampus. *Preprint*, 2018.

[2] Mojtaba Chehelcheraghi, Chie Nakatani, Erik Steur, and Cees van Leeuwen. A neural mass model of phase–amplitude coupling. *Biological cybernetics*, 110(2-3):171–192, 2016.

[3] Mojtaba Chehelcheraghi, Cees van Leeuwen, Erik Steur, and Chie Nakatani. A neural mass model of cross frequency coupling. *PloS one*, 12(4):e0173776, 2017.

[4] Eric R Kandel, James H Schwartz, Thomas M Jessell, Department of Biochemistry, Molecular Biophysics Thomas Jessell, Steven Siegelbaum, and AJ Hudspeth. *Principles of neural science*, volume 4. McGraw-hill New York, 2000.

[5] Juan A De Carlos and José Borrell. A historical reflection of the contributions of cajal and golgi to the foundations of neuroscience. *Brain research reviews*, 55(1):8–16, 2007.

[6] Santiago Ramón y Cajal. *Estructura de los centros nerviosos de las aves*. 1888.

[7] Jeffrey L Teeters, Kenneth D Harris, K Jarrod Millman, Bruno A Olshausen, and Friedrich T Sommer. Data sharing for computational neuroscience. *Neuroinformatics*, 6(1):47–55, 2008.

[8] Alan L Hodgkin and Andrew F Huxley. A quantitative description of membrane current and its application to conduction and excitation in nerve. *The Journal of physiology*, 117(4):500–544, 1952.

[9] Eugene M Izhikevich. Which model to use for cortical spiking neurons? *IEEE transactions on neural networks*, 15(5):1063–1070, 2004.

[10] Walter Freeman. *Neurodynamics: an exploration in mesoscopic brain dynamics*. Springer Science & Business Media, 2012.

[11] Gustavo Deco, Viktor K Jirsa, Peter A Robinson, Michael Breakspear, and Karl Friston. The dynamic brain: from spiking neurons to neural masses and cortical fields. *PLoS computational biology*, 4(8):e1000092, 2008.

[12] Olivier David and Karl J Friston. A neural mass model for meg/eeg:: coupling and neuronal dynamics. *NeuroImage*, 20(3):1743–1755, 2003.

[13] Hugh R Wilson and Jack D Cowan. Excitatory and inhibitory interactions in localized populations of model neurons. *Biophysical journal*, 12(1):1–24, 1972.

[14] FH Lopes Da Silva, A Van Rotterdam, P Barts, E Van Heusden, and W Burr. Models of neuronal populations: the basic mechanisms of rhythmicity. *Perspectives of brain research*, 45:281–308, 1976.

[15] F Wendling, F Bartolomei, JJ Bellanger, and P Chauvel. Epileptic fast activity can be explained by a model of impaired gabaergic dendritic inhibition. *European Journal of Neuroscience*, 15(9):1499–1508, 2002.

[16] Rosalyn J Moran, Stefan J Kiebel, Klaas E Stephan, RB Reilly, Jean Daunizeau, and Karl J Friston. A neural mass model of spectral responses in electrophysiology. *NeuroImage*, 37(3):706–720, 2007.

[17] Mauro Ursino, Filippo Cona, and Melissa Zavaglia. The generation of rhythms within a cortical region: analysis of a neural mass model. *NeuroImage*, 52(3):1080–1094, 2010.

[18] What is an action potential? `https://www.moleculardevices.com/applications/patch-clamp-electrophysiology/what-action-potential#gref`. Accessed: 2018-09-01.

[19] Per Andersen, Richard Morris, David Amaral, John O'Keefe, and Tim Bliss. *The hippocampus book*. Oxford university press, 2007.

[20] Yangling Mu and Fred H Gage. Adult hippocampal neurogenesis and its role in alzheimer's disease. *Molecular neurodegeneration*, 6(1):85, 2011.

[21] Stephan Heckers. Neuroimaging studies of the hippocampus in schizophrenia. *Hippocampus*, 11(5):520–528, 2001.

[22] Paul Gerrard and Robert Malcolm. Mechanisms of modafinil: a review of current research. *Neuropsychiatric disease and treatment*, 3(3):349, 2007.

[23] William Dement and Nathaniel Kleitman. Cyclic variations in eeg during sleep and their relation to eye movements, body motility, and dreaming. *Electroencephalography and clinical neurophysiology*, 9(4):673–690, 1957.

[24] Francisco Varela, Jean-Philippe Lachaux, Eugenio Rodriguez, and Jacques Martinerie. The brainweb: phase synchronization and large-scale integration. *Nature reviews neuroscience*, 2(4):229, 2001.

[25] Andreas K Engel and Wolf Singer. Temporal binding and the neural correlates of sensory awareness. *Trends in cognitive sciences*, 5(1):16–25, 2001.

[26] Antoine Lutz, Lawrence L Greischar, Nancy B Rawlings, Matthieu Ricard, and Richard J Davidson. Long-term meditators self-induce high-amplitude gamma synchrony during mental practice. *Proceedings of the National academy of Sciences of the United States of America*, 101(46):16369–16373, 2004.

[27] Xia Zhang, Wen-Juan Huang, and Wei-Wei Chen. Microwaves and alzheimer's disease. *Experimental and therapeutic medicine*, 12(4):1969–1972, 2016.

[28] William A Phillips and Steven M Silverstein. Convergence of biological and psychological perspectives on cognitive coordination in schizophrenia. *Behavioral and Brain Sciences*, 26(1):65–82, 2003.

[29] Ole Jensen and Laura L Colgin. Cross-frequency coupling between neuronal oscillations. *Trends in cognitive sciences*, 11(7):267–269, 2007.

[30] Anatol Bragin, Gábor Jandó, Zoltán Nádasdy, Jamille Hetke, K Wise, and Gy Buzsáki. Gamma (40-100 hz) oscillation in the hippocampus of the behaving rat. *Journal of Neuroscience*, 15(1):47–60, 1995.

[31] György Buzsáki. Theta oscillations in the hippocampus. *Neuron*, 33(3):325–340, 2002.

[32] Nikolai Axmacher, Melanie M Henseler, Ole Jensen, Ilona Weinreich, Christian E Elger, and Juergen Fell. Cross-frequency coupling supports multi-item working memory in the human hippocampus. *Proceedings of the National Academy of Sciences*, page 200911531, 2010.

[33] Haiteng Jiang, Ali Bahramisharif, Marcel AJ van Gerven, and Ole Jensen. Measuring directionality between neuronal oscillations of different frequencies. *Neuroimage*, 118:359–367, 2015.

[34] Ryan T Canolty, Erik Edwards, Sarang S Dalal, Maryam Soltani, Srikantan S Nagarajan, Heidi E Kirsch, Mitchel S Berger, Nicholas M Barbaro, and Robert T Knight. High gamma power is phase-locked to theta oscillations in human neocortex. *science*, 313(5793):1626–1628, 2006.

[35] Viktor Jirsa and Viktor Müller. Cross-frequency coupling in real and virtual brain networks. *Frontiers in computational neuroscience*, 7:78, 2013.

[36] Víctor J Lopez-Madrona. Matlab toolbox for cross-frequency coupling and cross-frequency directionality.

[37] Adriano BL Tort, Robert Komorowski, Howard Eichenbaum, and Nancy Kopell. Measuring phase-amplitude coupling between neuronal oscillations of different frequencies. *Journal of neurophysiology*, 104(2):1195–1210, 2010.

[38] Jessica A Cardin, Marie Carlén, Konstantinos Meletis, Ulf Knoblich, Feng Zhang, Karl Deisseroth, Li-Huei Tsai, and Christopher I Moore. Driving fast-spiking cells induces gamma rhythm and controls sensory responses. *Nature*, 459(7247):663, 2009.

[39] Alejandro Javier Pernía-Andrade and Peter Jonas. Theta-gamma-modulated synaptic currents in hippocampal granule cells in vivo define a mechanism for network oscillations. *Neuron*, 81(1):140–152, 2014.

[40] François Grimbert and Olivier Faugeras. Bifurcation analysis of jansen's neural mass model. *Neural computation*, 18(12):3052–3068, 2006.

[41] Lucia Wittner and Richard Miles. Factors defining a pacemaker region for synchrony in the hippocampus. *The Journal of physiology*, 584(3):867–883, 2007.

[42] Samuel A Neymotin, Maciej T Lazarewicz, Mohamed Sherif, Diego Contreras, Leif H Finkel, and William W Lytton. Ketamine disrupts theta modulation of gamma in a computer model of hippocampus. *Journal of Neuroscience*, 31(32):11733–11743, 2011.

[43] Samuel A Neymotin, Markus M Hilscher, Thiago C Moulin, Yosef Skolnick, Maciej T Lazarewicz, and William W Lytton. Ih tunes theta/gamma oscillations and cross-frequency coupling in an in silico ca3 model. *PLoS One*, 8(10):e76285, 2013.